CONTINUUM FLOW MODELS

REVISED BY **H. MICHAEL ZHANG***

ORIGINAL TEXT BY **REINHART KUHNE**[7]

PANOS MICHALOPOULOS[8]

* Professor, Department of Civil and Environmental Engineering, University of California Davis, One Shields Avenue, Davis, CA 95616

[7] Managing Director, Steierwald Schonharting und Partner, Hessbrühlstr. 21c 7 70565 Stuttgart, Germany

[8] Professor, Department of Civil Engineering, University of Minnesota Institute of Technology, 122 Civil Engineering Building, 500 Pillsbury Drive S.E., Minneapolis, MN 55455-0220

CHAPTER 5 - Frequently used Symbols

a	=	dimensionless traffic parameter
A	=	stop-start wave amplitude
α	=	sensitivity coefficient
b	=	net queue length at traffic signal
c	=	$g + r$ = cycle length
c_{0_2}	=	coefficient
c_0^2	=	constant, independent of density k
ds	=	infinitesimal time
Δt, Δx	=	the time and space increments respectively such that $\Delta x/\Delta t >$ free flow speed
$\delta\eta_i$, $\delta\eta_{i+1}$	=	deviations
η	=	state vector
η_i, η_{i+1}	=	state vector at position i, i+1
$f(x, v, t)$	=	vehicular speed distribution function
f	=	relative truck portion, $k_{pass} = k$
f_0	=	equilibrium speed distribution
Γ	=	fluctuating force as a stochastic quantity
g	=	effective green interval
g_j^n	=	is the generation (dissipation) rate at node j at $t = t_0 + n\Delta t$; if no sinks or sources exist g_j^n = 0 and the last term of Equation 5.28 vanishes
$g_{\min}$	=	minimum green time required for undersaturation
h	=	average space headway
i	=	station
j	=	node
k	=	density
k_-, k_+	=	density downstream, upstream shock
k_0	=	operating point
k_{10}	=	equilibrium density
K_A	=	constant value
k_a	=	density within L_2
k_{bumper}	=	density "bumper to bumper"
k_d, q_d	=	density, flow downstream
k_u, q_u	=	density, flow upstream
k_{hom}	=	vehicle density in homogeneous flow
k_j	=	jam density of the approach under consideration
k_j^n, q_j^n	=	density and flow rate on node j at $t = t_0 + n\Delta t$
k_m	=	density conditions
k_{pass}	=	density "bumper to bumper" for 100% passenger cars
k_{ref}	=	reference state
k_{truck}	=	density "bumper to bumper" for 100% trucks
L	=	distance
L	=	length of periodic interval
ld	=	logarithmus dualis
l_o	=	characteristic length
λ	=	wave length of stop-start waves
μ_0	=	dynamic viscosity
μ	=	viscosity term
n	=	current time step
N	=	normalization constant
n_i, n_2	=	exponents
N_i	=	number of cars (volume)
ω	=	eigenvalue
p	=	probability
q	=	actual traffic volume, flow
Q_0	=	net flow rate
q_a	=	average flow rate
$q_a k_a$	=	arrival flow and density conditions
q_{ni}	=	capacity flow
r	=	effective red interval
σ_0	=	quantity
T	=	oscillation time
t	=	time
t_0	=	the initial time
τ	=	relaxation time as interaction time lag
u	=	speed
$U_e(k)$	=	equilibrium speed-density relation
$u_e(k^n_{ij})$	=	equilibrium speed
u_f	=	free-flow speed of the approach under consideration
u_g	=	group velocity
$u_{max} - u_{min}$	=	speed range
u_w	=	shock wave speed
u_z	=	spatial derivative of profile speed
$v(k)$	=	viscosity
v_g	=	values of the group velocity
$W(q)$	=	distribution of the actual traffic volume values q
x	=	space
xh	=	estimated queue length
x_i, t_i, y_i	=	coordinates at point i
X_{ij}	=	length of any line ij
y	=	street width
$y(t)$	=	queue length at any time point t
y_{ij}	=	queue length from i to j assuming a positive direction opposite to x, i.e. from B to A
z	=	$x - U, t$, collective coordinate
$\dot{x}$	=	shockspeed

5. CONTINUUM FLOW MODELS

Original text by Reinhart Kühne and Panos Michalopoulos
Revised by H. M. Zhang

1 Conservation and traffic waves

There have been two kinds of traffic flow theories presented thus far in this monograph. Chapter 2 discussed the relations among aggregated quantities of flow rate, concentration and mean speeds for stationary vehicular traffic (these relations are also referred to as the equations of state in traffic flow), and Chapter 3 described the dynamic evolution of microscopic quantities of vehicle spacing, headway and speeds in single-lane traffic through the follow-the-leader type of models. In this Chapter we study another kind of traffic flow theory—continuum traffic flow theory—that describes the temporal-spatial evolution of macroscopic flow quantities as mentioned earlier. Continuum theories are natural extensions to the first two kinds of theories because, one one hand, they are closely related to the equations of state and car-following theories, and on the other hand, they overcome some of the drawbacks of the first (stationarity) and second (too much detail and limited observability) kinds of theories. The quantities and features that continuum theories describe, such as traffic concentration and shock waves, are mostly observable with current surveillance technology, which makes it easier to validate and calibrate these models.

Many theories exist in the continuum description of traffic flow. All of them share two fundamental relations: one is the conservation of vehicles and the other is the flow-concentration-speed relation

$$q = ku. \tag{1}$$

The $q - k - u$ relation is true by choice, i.e., one defines flow rate (q), concentration (k) and mean speed (u) in such a way that (1) always holds (see Chapter 2 for definitions). Conservation of vehicles, on the other hand, is true regardless of how q, k, u are defined, and can be expressed in different forms. Here we present three forms of the conservation law using variables in (1).

The first integral form of the conservation law. Consider a stretch of highway between x_1 and x_2 ($x_1 < x_2$). At time t the traffic concentration on this section is $k(x, t)$, and traffic flows into the section at a rate of $q(x_1, t)$, and out of the section at a rate of $q(x_2, t)$. The total number of

vehicles in this section at time t is then

$$\int_{x_1}^{x_2} k(x,t)dx.$$

Suppose no entries and exits exist between x_1 and x_2, then by conservation the rate of change in the number of vehicles

$$\frac{\partial}{\partial t}\int_{x_1}^{x_2} k(x,t)dx.$$

should equal to the net flow into this section

$$q(x_1,t) - q(x_2,t),$$

that is,

$$\frac{\partial}{\partial t}\int_{x_1}^{x_2} k(x,t)dx = q(x_1,t) - q(x_2,t), \tag{2}$$

This is the first integral form of the conservation law.

The second integral form of the conservation law. The conservation of vehicles also means that, in the $x-t$ plane, the net number of vehicles passing through any closed curve is zero provided that no sources and sinks are there in the enclosed region (Fig. 2). Note that the number of vehicles across any segment dl of curve $\mathcal{C}$ is $-kdx + qdt$, the total number of vehicles across the enclosed region is therefore the line integral of the vector field $(-k, q)$, and we have the second integral form of the conservation law:

$$\int_{\mathcal{C}} -kdx + qdt = 0. \tag{3}$$

(3) implies that we can construct a scalar function $N(x,t)$ with the properties

$$q = \frac{\partial N}{\partial t},\ k = -\frac{\partial N}{\partial x}.$$

This function is the cumulative count of vehicles passing location x at time t, provided that $N(x, t = 0) = 0$. The fact that such a function exists is another consequence of the conservation law.

The differential form of the conservation law. By applying the divergence theorem to the second integral form we obtain

$$\int_{\mathcal{C}} -kdx + qdt = \int\int_D \left(\frac{\partial k}{\partial t} + \frac{\partial q}{\partial x}\right) dxdt = 0,$$

which leads to the differential form of the conservation law:

$$\frac{\partial k}{\partial t} + \frac{\partial q}{\partial x} = 0. \tag{4}$$

The three different forms of the conservation law are not completely equivalent. Note that in the differential form, both k and q are required to be differentiable with respect to time t and space x. In contrast, it is perfectly fine in the integral forms that these variables are discontinuous in space and/or time. This is an important distinction because a special kind of traffic waves, called shock waves, are prevalent in vehicular traffic flow and play an essential role in the continuum

description of traffic flow. A shock wave is a drastic change in traffic concentration (and/or speed, flow rate) that propagates through a traffic stream. Examples of shock waves include the stoppage of traffic in front of a red light, and traffic slow-downs caused by an accident. In reality a shock always has a profile (that is, a transition region of non-zero width) that usually spans a few vehicle lengths, but this can be practically treated as a discontinuity when compared with the length of roads in consideration.

Because of the existence of shocks, it is necessary to expand the solution space of (4) to include the so-called *weak solutions*. In mathematical sense a weak solution is a function $(k, q)(x, t)$ that satisfies (4) everywhere except along a certain path $x(t)$. On $x(t)$ $(k, q)(x, t)$ are discontinuous but obey the integral forms of the conservation law. A shock wave solution to (4) is a weak solution. Moreover, its path $x(t)$ is governed by the following equation:

$$\dot{x}(t) = [q]/[k]. \tag{5}$$

where $[k] = k_r - k_l, [q] = q_r - q_l$, $\dot{x}(t)$ is the speed of the shock, also denoted as s, and $(k_{l,r}, q_{l,r})$ are the traffic states immediately to the right and left of the shock path $x(t)$, respectively. Expression (5) is also known as the Rankine-Hugoniot (R-H) condition (LeVeque 1992) , which is a consequence of the conservation law.

Expression (5) has a simple geometric interpretation in the (k, q) plane, also known as the $k-q$ phase plane. It is simply the slope of the segment that connects the two phase points (k_l, q_l) and (k_r, q_r) (Fig. 1(a)). Suppose that a unique curve connects $(k_{l,r}, q_{l,r})$, and $k_r \to k_l$ (i.e., the shock is weak), then s approaches the slope of the tangent of the connecting curve at (k_l, q_l) (Fig. 1(b)). We call this speed the speed of *traffic sound waves*, and give it a special notation $c(k)$. This is the speed that information is propagated in homogeneous traffic. It plays a central role in the basic kinematic wave model of traffic flow. It must be pointed out that a unique $q - k$ curve is not necessary to compute the shock speed. This can be done as long as both the densities and flow rates on both sides of the shock are known.

Next we provide two derivations of (5) from the conservation law. The first derivation is based on the first integral form of the conservation law. Suppose that traffic states on both sides of the shock are constant states $(k_{1,2}, q_{1,2})$, and suppose that two observers located at $x_1(t)$ and $x_2(t)$ on the two sides of the shock (i.e., $x_1 < x(t) < x_2$) travel at precisely the speed of the shock, s. We apply the conservation law (2) to the region between the two observers after doing a coordinate transformation $x^{'} = x - st$ to obtain:

$$\frac{\partial}{\partial t} \int_{x_1^{'}}^{x_2^{'}} k(x, t)dx = [q_1 - k_1 s] - [q_2 - k_2 s].$$

The integral, however, can be evaluated independently in $[x_1^{'}, x_l^{'})$ and $(x_r^{'}, x_2^{'}]$, where $x_{l,r}^{'}$ are points immediate to the right/left of shock path $x^{'}(t)$. This integral turns out to be

$$k_1(x_l^{'} - x_1^{'}) + k_2(x_2^{'} - x_r^{'}),$$

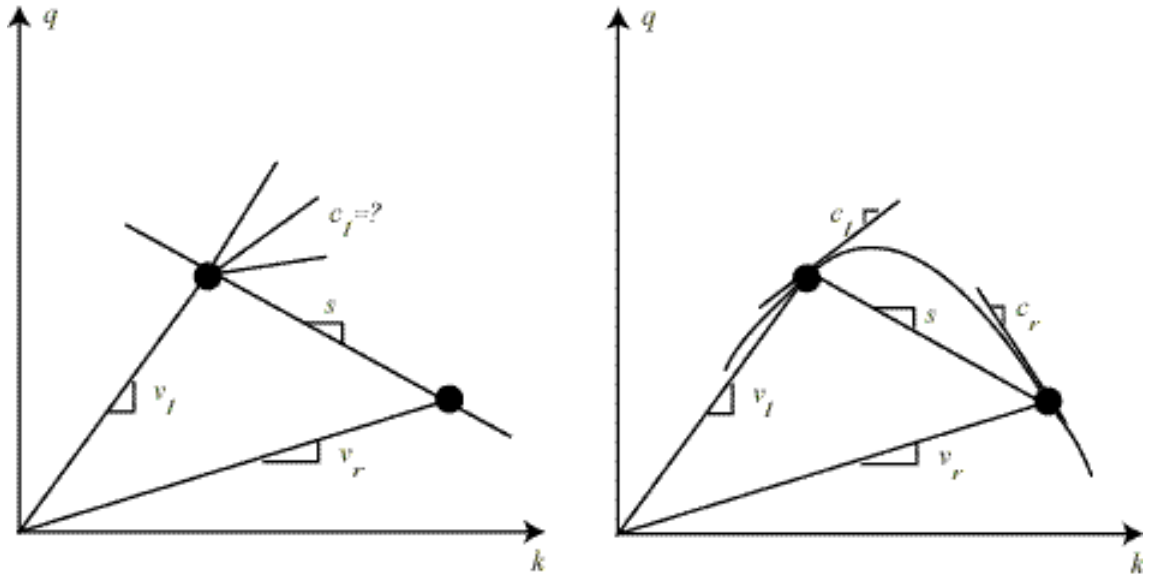

Figure 1: Geometric representation of shocks, sound waves, and traffic speeds in the $k-q$ phase plane

a constant, whose derivative is zero. Therefore we have

$$[q_1 - k_1 s] - [q_2 - k_2 s] = 0,$$

which leads to (5) after rearranging terms.

The second derivation of the Rankine-Hugoniot condition comes from the second integral form. As shown in Fig.2, a shock path $x(t)$ breaks the closed curve $\mathcal{C}$ into two parts $\mathcal{C}_l$ and $\mathcal{C}_r$. Let $\Gamma_{l,r}$ be the right/left edges of $x(t)$, respectively, then the conservation law applies to each of the three enclosures $\mathcal{C}$, $\mathcal{C}_l \cup \Gamma_l$, and $\mathcal{C}_r \cup \Gamma_r$:

$$\int_{\mathcal{C}} -kdx + qdt = 0. \tag{6}$$

$$\int_{\mathcal{C}_l \cup \Gamma_l} -kdx + qdt = 0. \tag{7}$$

$$\int_{\mathcal{C}_r \cup \Gamma_r} -kdx + qdt = 0. \tag{8}$$

Adding (7) and (8) together and rearranging terms we obtain

$$\int_{\mathcal{C}} -kdx + qdt + \int_{\Gamma_l} -kdx + qdt + \int_{\Gamma_r} -kdx + qdt = 0.$$

The first integral is zero, and the second and third integrand become

$$(-k_{l,r} s + q_{l,r})dt$$

on $\Gamma_{l,r}$. Taking account the direction of integration we obtain the following integral equation:

$$\int_{t_1}^{t_2} \{(-k_l s + q_l) - (-k_r s + q_r)\} dt = 0.$$

This implies that

$$(-k_l s + q_l) - (-k_r s + q_r) = 0,$$

which also leads to the Rankine-Hugoniot shock condition.

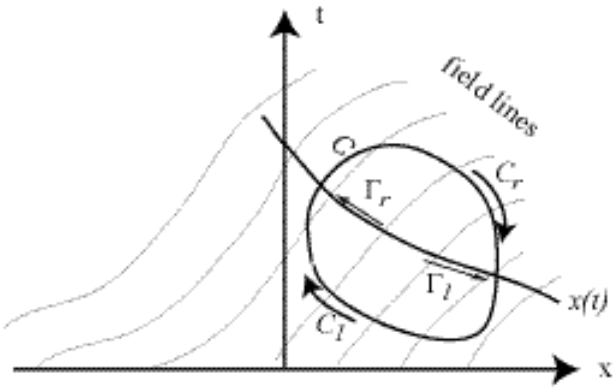

Figure 2: Field representation of shocks and conservation of flow

The differential conservation law (4), supplemented by the Rankine-Hugoniot condition (5), is the corner stone of all continuum vehicular traffic theories. Yet it is not a complete theory, nor is it unique to traffic flow. In fact, the differential conservation law is obeyed by many kinds of material fluids, such as gas flow in a pipe or water flow in a channel. As such, it does not capture the unique characters of vehicular traffic flow, a special kind of "fluid". It must be supplemented by additional relations to form a complete and useful traffic flow theory. Some of the relations between macroscopic traffic variables are already available and have been discussed in Chapter 2. These are the binary relations between flow rate, traffic concentration and mean travel speed. Although these relations are found among stationary traffic, they can also be used as a first approximation of dynamic flow-concentration-speed relations. This leads to the first, and the simplest continuum theory of traffic flow—the kinematic wave theory developed independently by Lighthill and Whitham (1955), and Richards (1956) (The LWR model). A more accurate relation between flow-concentration or speed-concentration is one that accounts for the dynamic behavior of drivers—anticipation and inertia. The usage of such a relation leads to the so-called higher-order models. We will study in this chapter these two kinds of continuum theories in great deal. In the sections to follow, we'll first study the properties of the LWR model and its Riemann problem, then study the properties of a special class of higher-order models and their respective Riemann problems. Next we develop numerical approximations of both types of models, and finally we provide some examples of the use of the numerical approximations.

2 The kinematic wave model of LWR

2.1 The LWR model and characteristics

The LWR model assumes that the relation observed in *stationary* flow, $q = f_*(k)$, also applies to dynamic traffic. With such a relation, the conservation law becomes:

$$k_t + f_*(k)_x = 0. \tag{9}$$

and the Rankine-Hugoniot condition becomes

$$s = [f_*]/[k].$$

This is the celebrated kinematic wave model of LWR. It is one of the simplest nonlinear scalar conservation laws in physics and engineering.

Experimental evidence indicates that $f_*(k)$ is usually smooth and concave (refer to Chapter 2), and satisfies the following boundary conditions:

$$f_*(0) = f_*(k_j) = 0,$$

$$f_*^{'}(0) = v_f > 0,\ f_*{}'(k_j) = c_j < 0.$$

where k_j is the jam concentration at which vehicles grind to a halt, usually ranging from 260 vpm to 330 vpm (in passenger car units), c_j is the speed of traffic sound waves at jam condition, taking values in the range of [-10 mph, -20 mph], and v_f is free-flow travel speed, ranging from $55mph$ to $75mph$ on freeways. All these parameter values are readily computable from conventional field measurements.

With the introduction of traffic wave speed (when no confusion arises we use traffic wave and traffic sound waves interchangably) $c(k) = f_*{}'(k)$, the LWR model also reads

$$k_t + c(k)k_x = 0. \tag{10}$$

Now let us look at what changes in concentration an observer sees when he travels at the speed of $c(k)$, that of traffic waves.

$$\frac{dk}{dt} = k_t + k_x\frac{dx}{dt} = k_t + c(k)k_x = 0.$$

That is to say, he sees no changes in density at all if he travels at the wave speed. As a result, if he knows the initial concentration at a point ξ, he'll know the concentration at any point on the path

$$\dot{x}(t) = c(k),\ x(0) = \xi. \tag{11}$$

This path is called the *characteristic curve* of the LWR model, and the wave speed $c(k)$ is also known as the *characteristic speed* of the LWR model. Because k is constant along the characteristic curve, the characteristic of (9) is therefore a straight line.

One must not confuse over traffic sound wave speeds, shock wave speeds, characteristic speeds, and vehicle speeds. Traffic sound wave speeds and characteristic speeds in the LWR model are

identical, which are the slopes of the tangential lines on the flow-concentration curve (also known as *the fundamental diagram* of traffic flow). Shock wave speeds are the slopes of the secant that connecting any two traffic states on $f_*(k)$, and vehicular speeds are the slopes of the rays from the origin to points on $f_*(k)$ (Fig. 1). Because of the concave shape of $f_*(k)$, we have the following relations among the various speeds:

$$v = f_*/k \equiv v_*(k) \geq c(k),\ s < v_*(k_{l,r}),$$

that is to say, all waves, including sound and shock waves, travel no faster than traffic. In other words, information in LWR traffic is propagated against the traffic stream. This property of information propagation in the LWR model is known as the *anisotropic property* of traffic flow. The anisotropic property may not hold if the fundamental diagram is not concave (Zhang 2000c).

2.2 The Riemann problem and entropy solutions

The LWR model is a well-posed hyperbolic partial differential equation (pde) [1] and can be solved with proper initial/boundary data. In fact, analytical solutions can be obtained for a special kind of problem called Riemann problem, whose initial data—the so-called Reimann data—are two constant states $k_{l,r} \geq 0$ separated by a single jump:

$$k(x, t=0) = \begin{cases} k_l, & x < 0, \\ k_r, & x > 0 \end{cases}$$

The analytical solution to the Riemann problem can either be a shock:

$$k(x,t) = \begin{cases} k_l, & x < st, \\ k_r, & x > st. \end{cases} \tag{12}$$

or a smooth expansion wave (also known as a rarefaction wave):

$$k(x,t) = \begin{cases} k_l, & x < c_l t, \\ (f_*')^{-1}\left(\frac{x}{t}\right), & c_l t \leq x \leq c_r t, \\ k_r, & x > c_r t \end{cases} \tag{13}$$

The condition for it to be a shock is governed by the so-called *entropy* condition, which states that

$$c_l > c_r. \tag{14}$$

Otherwise the solution will be an expansion wave. Because of the concavity condition $f_*''(k) < 0$, (14) implies that $k_l < k_r$, that is, shocks arising from the LWR theory are compressive. Moreover, they reach vehicles from upstream because $s < v_{l,r}$. Examples of the two kinds of solutions to a Riemann problem are shown in Figs. 3& 4.

For general initial conditions, it is usually tedious, if not difficult, to obtain analytical solutions of the LWR equation, and numerical approximations are often sought, where the Riemann problem

[1] A pde is hyperbolic if its characteristic speeds are real (as compared to imaginary).

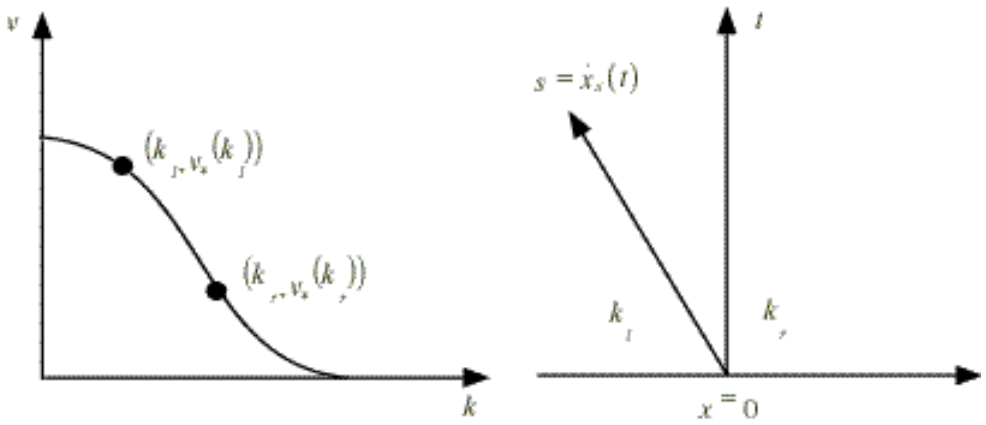

Figure 3: A shock solution

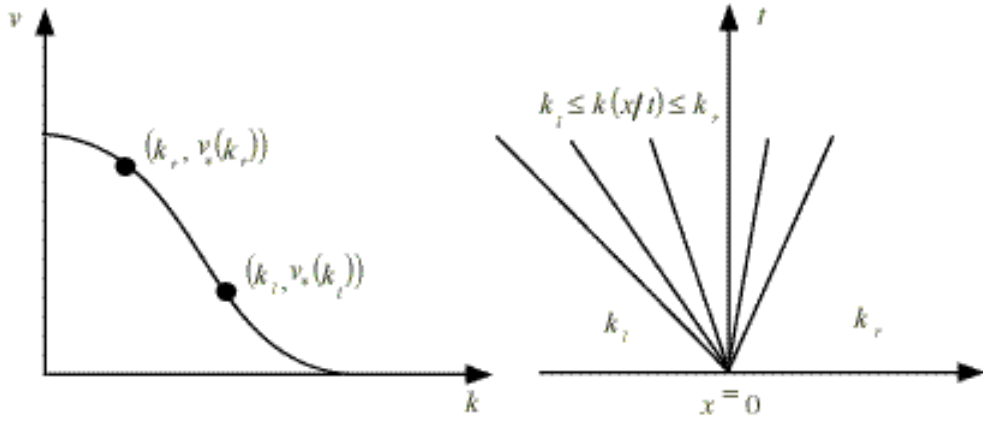

Figure 4: A rarefaction solution

plays a key role in developing some of the most efficient and accurate numerical schemes. This will be discussed in Section 4 together with the treatment of boundary conditions. There are special cases where an analytical solution is still straightforward to obtain. One case involves a special kind of initial condition—$k(x,0)$ is piece-wise constant and and increasing, and another case involves a special kind of fundamental diagram—the triangular shaped fundamental diagram that has only two wave speeds (Koshi et al 1983, Newell 1993). In the former case, a series of Riemann problems can be solved with consideration of wave interactions, and in the latter case, expansion waves are replaced by acceleration shocks, and it is much simpler to construct the solutions with shocks than expansion waves (see Newell 1993).

2.3 Applications

Same as Sections 5.1.3 & 5.1.4 in the original text.

2.4 Extensions to the LWR model

The LWR model we presented applies to traffic on a homogeneous highway with no entering and exiting traffic. In reality all highways have entries and exits and variable geometric features. Fortunately the LWR equation can be easily extended to model such inhomogeneities.

Suppose the net inflow to a road section is $s(x,t)dxdt$ from sources such as freeway ramps, then from conservation we have

$$k_t + f_*(k)_x = r(x,t), \tag{15}$$

This is the LWR model with sources. These source flows can be entering or exiting flows from ramps, or both.

When road geometries change, such as the drop of a lane at some locations, they often generate disturbances that cause traffic breakdowns. The effect of such inhomogeneities on traffic flow can be captured to some degree with a location-dependent fundamental diagram, $f_*(k,x)$. Because vehicle conservation still holds, applying the conservation principle to an inhomogeneous road leads to the following extended LWR model:

$$k_t + f_*(k,x)_x = 0. \tag{16}$$

If a road segment has both sources and geometric inhomogeneities, the following model applies:

$$k_t + f_*(k,x)_x = r(x,t). \tag{17}$$

Like the homogeneous LWR model, these extensions are also non-linear hyperbolic pdes, whose characteristics are

$$\dot{x} = f_{*k}(k,x). \tag{18}$$

These characteristics, however, are no longer straight lines as in the homogeneous model. This is because along the characteristics, we have

$$\dot{k} = k_t + k_x\dot{x} = k_t + f_{*k}k_x = \begin{cases} r, & \text{for (15)} \\ -f_{*x}, & \text{for (16)} \\ r - f_{*x}, & \text{for (17)} \end{cases} \tag{19}$$

(18) and (19) form a system of ordinary differential equations (ode), and can be solved iteratively using any ode solver such as the Runge-Kutta method. This way of solving the inhomogeneous LWR models is known as *the method of characteristics* (Courant and Hilbert 1962).

The basic LWR model and its various extensions we have covered treat traffic across lanes as homogeneous, which is somewhat restrictive because alternate motion of traffic in different lanes is often observed in heavily congested traffic. This limitation is easily overcome by modeling traffic evolution in each lane. Here the conservation principle still applies, but a continuum of sources exist for each lane. These sources are the exchange of flow between adjacent lanes. Without loss of generality, assume a two-lane highway with traffic $(k_1(x,t), q_1(x,t))$ and $(k_2(x,t), q_2(x,t))$. Let Q_1 be the net amount of traffic entering lane 1 from lane 2 in unit time and distance, and Q_1 be

the net amount of traffic entering lane 2 from lane 1 in unit time and distance, then the extended LWR model for a two-lane highway is (Dressler 1949)

$$k_{1t} + q_{1x} = Q_1, \tag{20}$$

$$k_{2t} + q_{2x} = Q_2. \tag{21}$$

where $q_1 = f_{1*}(k_1)$ and $q_2 = f_{2*}(k_2)$.

From conservation we know the source flows $Q_1,\ Q_2$ observe

$$Q_1 + Q_2 = 0$$

and experiences tell us that the change of flow between lanes is related to the differential of lane speeds/densities, for drivers always like to move into the faster lane in congested traffic. An example of $Q_1,\ Q_2$ was proposed by Gazis et al. (1962):

$$Q_{1,2} = \alpha[(k_{2,1} - k_{1,2}) - (k^0_{2,1} - k^0_{1,2})] \tag{22}$$

where $k^0_{1,2}$ are equilibrium densities of lanes 1 & 2, respectively (Gazis et al. 1962). These can be observed experimentally.

The above lane-specific LWR model is a system of quasi-linear PDEs and can be expressed in vector forms

$$\begin{pmatrix} \mathrm{k}_1 \\ \mathrm{k}_2 \end{pmatrix}_t + \begin{pmatrix} \mathrm{f}_{1*}(k_1) \\ \mathrm{f}_{2*}(k_2) \end{pmatrix}_x = \begin{pmatrix} \mathrm{Q}_1(k_1, k_2) \\ \mathrm{Q}_2(k_1, k_2) \end{pmatrix}, \tag{23}$$

or

$$\begin{pmatrix} \mathrm{k}_1 \\ \mathrm{k}_2 \end{pmatrix}_t + \begin{pmatrix} f_{1*,k_1} & 0 \\ 0 & f_{2*,k_2} \end{pmatrix} \begin{pmatrix} \mathrm{k}_1 \\ \mathrm{k}_2 \end{pmatrix}_x = \begin{pmatrix} \mathrm{Q}_1(k_1, k_2) \\ \mathrm{Q}_2(k_1, k_2) \end{pmatrix}. \tag{24}$$

For a system of quasi-linear PDEs, the characteristics are the eigenvalues of the Jacobian matrix $DF \equiv \begin{pmatrix} f_{1*,k_1} & 0 \\ 0 & f_{2*,k_2} \end{pmatrix}$, which contains the partial derivatives of the flow vector $F(U) \equiv \begin{pmatrix} \mathrm{f}_{1*}(k_1) \\ \mathrm{f}_{2*}(k_2) \end{pmatrix}$ with respect to the state vector $U \equiv \begin{pmatrix} \mathrm{k}_1 \\ \mathrm{k}_2 \end{pmatrix}$.

This system is said to be strictly hyperbolic if all its characteristics are real and distinct. It is easy to see that the characteristics of (23) are $f'_{1*}(k_1)$ and $f'_{2*}(k_2)$ because the dynamics of the two lanes are nearly decoupled (the only coupling comes from the source term). The system is strictly hyperbolic under the condition that $f_{1*}(k_1) \neq f_{2*}(k_2)$ and $f''_{1,2*} < 0$. Thus this system can be solved in the same way as other inhomogeneous models through the method of characteristics. Only this time one solves a system of four odes instead of two:

$$\dot{x}_1 = f'_{1*}(k_1),$$

$$\dot{x}_2 = f'_{2*}(k_2),$$

$$\dot{k}_1 = Q_1(k_1, k_2),$$

$$\dot{k}_2 = Q_2(k_1, k_2).$$

It should be noted that both the inhomogeneous models and the multiple-lane models can be solved numerically using the finite difference procedures developed in Section 5.

2.5 Limitations of the LWR model

The kinematic wave model of LWR is only a first approximation of the real traffic flow process and is deficient in describing a number of traffic features of potential importance. The include (i) driver differences, (ii) shock structure, (iii) forward moving waves in queued up traffic and (iv) traffic instability (Daganzo 1997).

The LWR model is inadequate for modeling light traffic because it does not recognize the segregation of fast and slow drivers in the traffic stream owing to passing. An adequate model for traffic where significant amount of passing takes place should track both fast and slow drivers and their interactions, not by lumping both types of drivers together through a single descriptor such as density $k(x,t)$. When drivers travel at roughly the same speed, however, the LWR model can still be used for light traffic, where density is independent of concentration and flow increases linearly with density.

The second deficiency of the LWR model lies in its treatment of shock waves. The shocks in the LWR model has no width, i.e., no transition region. A vehicle enters a shock thus dropping its speed in no time, implying an infinite deceleration. In reality, shocks always have a structure, i.e., a transition region of a few vehicles' length in which vehicles decelerate at finite rates. This deficiency can be addressed through introducing higher-order approximations of traffic dynamics (Kühne 1984,1989) or using a microscopic description (Newell 1961). It is one of the author's (Zhang) opinion that as long as the accurate knowledge of vehicle acceleration is not of main interest, the lack of a shock structure is not a major failing of the LWR theory, because in comparison with the space scale one is modeling, a few vehicle lengths of shock width can be practically considered as nil. To most applications, the important matter is whether the LWR theory gives a reasonable estimate of shock speeds. Empirical evidence indicates that it does (Chapter 4 in Daganzo 1997).

The LWR theory has only one family of waves which travels at a speed of $f_*^{'}(k)$. These waves always travel against the traffic stream because $f_*^{'}(k) < v_*(k)$. In particular, $f_*^{'}(k) < 0$ when concentration k exceeds a critical value k_* at which flow rate is maximal. An early study of tunnel traffic, however, revealed that a different type of waves exists in real traffic (Edie and Baverez 1967). In analyzing the tunnel traffic data, Edie and Baverez (1967) noted that " small changes in flow may not propagate at a speed equal to the slope of the tangent to a steady-state q-k curve as suggested by the hydrodynamic wave theories of traffic flow. Instead, they are carried along at about stream speed or only slightly less than stream speed right up to saturation flows, at which level they suddenly reverse directions." This observation indicates that apart from the family of waves that travels against the traffic stream, there's at least another family of traffic waves that travels with the traffic stream, even in congested traffic. The findings of Edie and Baverez (1967) prompted Newell (1965) to suggest a fundamental diagram with multiple branches—one branch for free flow, one for acceleration flow and another for deceleration flow. The extended LWR theory with this fundamental diagram was able to explain not only the forward wave motion in queued-up traffic, but also the instability found in tunnel traffic.

In comparison with other deficiencies of the LWR theory, the fourth deficiency, namely its

inability to model traffic instability, has more serious consequences, for traffic instability is at the very heart of the traffic congestion phenomenon. The LWR model is always stable in the sense that traffic disturbances, small or large, are always dampened. In other words, a driver who obeys the LWR driving law always responds to stimulus properly, i.e., he always manages to change his speed in the right amount of time and with the right magnitude that he simply absorbs the disturbance. In fact the reaction time of a LWR driver is zero and the rate of adjustment he makes is infinite. In reality, a driver responds to traffic events with a time delay, and not always precisely. As a result, some disturbances in real traffic may get magnified as they propagate through the traffic stream, causing traffic break-downs (stop-and-go) that could last for several hours. Such stop-and-go traffic patterns exhibit, in physical space (i.e., $x-t$ domain), periodic oscillations with amplitude-dependent oscillation time, and in phase space (i.e., $q-k$ or $k-u$ domain), hysteresis loops and wide scatter of data points.

Evidences of traffic instability and the resulting stop-and-go flow pattern are found on highways around the globe. Perhaps the most impressive measurements of transients and stop-start wave formation are gained from European freeways. Due to space restrictions, there are numerous freeways with two lanes per highway in Europe. These freeways, often equipped with a dense measurement grid not only for volume and occupancy but also for speed detection, show stable stop-start waves lasting in some cases for more than three hours. Measurement data exists for Germany (Leutzbach 1991), the Netherlands (Verweij 1985), and Italy (Ferrari 1989). First we examine the measurements from German highways. The German data were collected from the Autobahn A5 Karlsruhe-Basel at 617 km by the Institute of Transport Studies at Karlsruhe University (Kühne 1987). Each measurement point is a mean value of a two-minute ensemble actuated every 30 sec. These data were collected during a holiday when no trucks used that stretch of road.

All the data sets have traffic densities over the critical density and show signs of instability (i.e., stop-start waves with more or less regular shape and of long duration - in some series up to 12 traffic breakdowns). These data can characterized in the time domain by their oscillation times T and magnitudes A. These characteristic features derived from the data shown in **Figures 5.9a,b and 5.9c,d (in the original text)** (Kühne 1987,Michalopoulos and Pisharody 1980) are listed in the following table:

Table 1: Oscillation time and magnitudes of stop-and-go traffic from German measurement

oscillation time T	16 min	15 min	7.5 min	5 min
amplitude A	70km/h	70 km/h	40 km/h	25 km/h
measurement figure	2a	2b	3a	3b

These characteristic values show a proportionally between amplitude and oscillation time. This strong dependence is a sign for the non-linear and anharmonic character of stop-start waves. In the case of harmonic oscillations, the amplitude is independent of the oscillation time as the linear

pendulum shows. Obviously, the proportionally holds only for the range between traffic flow at a critical lane speed of about 80 km/h (= speed corresponding to the critical density kc . 25 veh/km) and creeping with jam speed of about 10 km/h. For oscillations covering the whole range between free-flow speed and complete gridlock, saturation effects will reduce the proportionally.

Examples of stop-start waves from other locations, such as the Netherlands (Verweij 1985), Japan (Koshi et al. 1983), Italy (Ferrari 1989) and the U.S.A. also show similar characters as those observed on German highways. Such oscillations, when viewed from the $q - k$ phase plane, show wider scatter of data points in the congested regime. Embedded in the scatter are sharp drops (often referred to as *the capacity drop*) and hysteresis loops (e.g., Treiterer and Myers 1974) of irregular shapes that differ from the equilibrium phase curve $q = f_*(k)$ and cannot be simply explained away by stochastic arguments. All but the first deficiencies of the LWR model can be addressed, to various degrees of success, through the introduction of higher-order approximations or "dynamic" fundamental diagrams. This leads to two classes of traffic flow models—higher-order and lower-order continuum models. Higher-order models introduce a dynamic speed-concentration or flow concentration relation that accounts for driver reaction time and anticipation of traffic conditions ahead, i.e.,

$$v(x, t + \tau) = V_*(k(x + \Delta x, t)),$$

$$q(x, t + \tau) = kV_*(k(x + \Delta x, t)).$$

The approximations of these dynamic relations lead to evolution equations for travel speed or flow rate (Payne 1971, Whitham 1974, Zhang 1998). Consequently the traffic model becomes a system of partial differential equations and its solutions, when shown in the phase plane, deviate from the equilibrium fundamental diagram, producing the scatter and forward waves in the congested region. Lower-order models, on the other hand, models different traffic motions—acceleration, deceleration and coasting—explicitly on the fundamental diagram. Their fundamental diagrams $f_*(k)$ has multiple branches and connecting curves, each describes a particular kind of motion (Newell 1965, Zhang 2001). For one reason or another, higher-order models are more widely studied and used than lower-order models. Therefore we will focus our presentation on higher-order models in the remaining text. Readers who are interested in lower-order traffic flow models can refer to Newell (1965), Daganzo (1999a,b) and Zhang (2001).

3 Higher-order continuum models

The development of higher-order traffic flow models again originated from the seminal work of Lighthill and Whitham (1955), in which they suggested the following higher-order extension of their first-order model:

$$\text{The LW model:} \qquad q_t + Cq_x + Tq_{tt} - Dq_{xx} = 0, \tag{25}$$

where C is convection speed, T is a reaction time constant and D is the diffusion coefficient. Because of a lack of strong experimental evidence in support of such an extension, higher-order

approximations of traffic flow were not pursued further till 1971, when Payne (1971) and later Whitham (1974) derived a so-called 'momentum equation' from a car-following argument:

$$kv_t + vv_x + \frac{c_0^2}{k}k_x = \frac{v_*(k) - v}{\tau}, \tag{26}$$

where $v_*(k)$ is the equilibrium speed-concentration relation, $c_0 < 0$ is the 'sound' speed, and is given by $c_0^2 = \frac{\mu}{\tau}$, where μ is often referred to as the anticipation coefficient and τ relaxation time [2]. Recently, Zhang (1998) proposed a new addition to the existing momentum equations:

$$v_t + vv_x + kv_*'(k)^2 k_x = \frac{v_*(k) - v}{\tau}, \tag{27}$$

which is structurally similar to the momentum equation of Payne (1971) and Whitham (1974).

On the left hand side of the momentum equations, the second term is the change of speed due to convection, and the third term captures drivers' adjustment to travel speeds owing to anticipation. The term on the right hand side captures drivers' affinity to equilibrium travel speeds. In the momentum equations, the acceleration of a vehicle, expressed by the material derivative $v_t + vv_x$, responds negatively to the increase of concentration downstream, and positively (negatively) to travel speeds that are lower (higher) than the corresponding equilibrium speeds for the same concentration. As a result, travel speed v in both momentum equations usually differs from the equilibrium speed $v_*(k)$ under the same traffic condition, but this difference is reduced over time because of relaxation effects. The parameter τ decides the strength of relaxation. In literature τ is often interpreted as driver reaction time, whose value ranges from 1 sec to 1.8 sec.

Through the definition of a concentration dependent sound speed $c(k)$ ($= kv_*'(k)$, or c_0, or $-\sqrt{\frac{\mu}{\tau}}$), both momentum equations can be expressed in a general form:

$$v_t + vv_x + \frac{c^2(k)}{k}k_x = \frac{v_*(k) - v}{\tau}. \tag{28}$$

This evolution equation of travel speed, coupled with the continuity equation

$$k_t + (kv)_x = 0, \tag{29}$$

forms what we call a generalized PW higher-order model. The general PW model comprises a system of partial differential equations that can be compactly expressed using vector notation

$$\begin{pmatrix} k \\ v \end{pmatrix}_t + \begin{pmatrix} v & k \\ \frac{c^2(k)}{k} & v \end{pmatrix} \begin{pmatrix} k \\ v \end{pmatrix}_x = \begin{pmatrix} 0 \\ \frac{v_* - v}{\tau} \end{pmatrix}. \tag{30}$$

or

$$U_t + A(U)U_x = R(U), \tag{31}$$

where $U = \begin{pmatrix} k \\ v \end{pmatrix}$, $A(U) = \begin{pmatrix} v & k \\ \frac{c^2(k)}{k} & v \end{pmatrix}$ and $R(U) = \begin{pmatrix} 0 \\ \frac{v_* - v}{\tau} \end{pmatrix}$.

[2] There are other versions of (26)that differ in values taken by μ. Payne (1971), for example, gives $\mu = -\frac{v_*'}{2}$

This system is strictly hyperbolic because its characteristics, the eigenvalues of the Jacobian matrix $A(U)$, are real and distinctive

$$\lambda_{1,2} = v \pm c(k),\ \lambda_1 < \lambda_2. \tag{32}$$

The same is true for the LW model, because, through introduction of two auxiliary variables $w = q_t$ and $z = q_x$ the LW model can be transformed into a system of PDEs

$$\begin{pmatrix} w \\ z \end{pmatrix}_t + \begin{pmatrix} 0 & 1 \\ -\frac{D}{T} & 0 \end{pmatrix} \begin{pmatrix} w \\ z \end{pmatrix}_x = -\begin{pmatrix} 0 \\ w + Cz \end{pmatrix}, \tag{33}$$

whose characteristics are

$$\lambda_{1,2} = \mp\sqrt{\frac{D}{T}},\ \lambda_1 < \lambda_2.$$

The two higher-order models differ, however, in that the general PW model is genuinely nonlinear while the LW model is linearly degenerate.

Although both the LWR model and the general PW model are hyperbolic, the latter has two characteristics, one is always slower than traffic and the other always faster than traffic, owing to $c(k) < 0$. This is constrasted to the single characteristic of the LWR model, $\lambda_* = v_*(k) + kv_*'(k)$ that is always slower than traffic. These differences have profound consequences on the behavior of these models, which we shall discuss in the context of various kinds traffic waves.

3.1 Propagation of traffic sound waves in higher-order models

We first note that traffic sound waves—the propagation of small disturbances in homogeneous traffic—travel at characteristic speeds in the LWR model. In higher-order models, there are two families of characteristics, thus two characteristic speeds. If a disturbance is still propagated at characteristic speeds, then it travels in both directions of traffic with different speeds, reaching drivers from front and behind. This can be checked through writing the higher-order model in question, here the LW model, in a special form

$$\left\{(\partial_t + C\partial_x) + \left(\partial_t + \sqrt{\frac{D}{T}}\partial_x\right)\left(\partial_t - \sqrt{\frac{D}{T}}\partial_x\right)\right\} q = 0.$$

where $\partial_t + () * \partial_x$ is called a wave operator.

From this special form, one can clearly see that the LW model possesses three families of waves: the first order wave traveling at the convection speed $c_* = C$ (which is also the characteristic speed of the corresponding first-order model $q_t + Cq_x = 0$), the slower second order wave traveling at the first characteristic speed $c_1 = -\sqrt{\frac{D}{T}}$ and the faster second order wave traveling at the speed of the second characteristic $c_2 = \sqrt{\frac{D}{T}}$. For certain parameter values of D and T, the second characteristic speed can be greater than the convection speed, indicating that fast waves reach traffic from behind (*the rear view mirror effect*). In fact, this is also required for LW traffic to be stable. Otherwise

the first-order signals would violate the second-order signals, which leads to traffic instability. The general stability condition for the above higher-order model is

$$c_1 \leq c_* \leq c_2, \tag{34}$$

that is, the first order waves are sandwiched between the two second order waves. This stability condition can be derived from Fourier stability analysis (e.g., Whitham 1974, Kühne 1984, Zhang 1999).

For the general PW model, small perturbations around equilibrium points (k_0, v_0) would propagate in the same way as the waves in the LW model, only with different wave speeds. Instead of $c_* = C,\ c_1 = -\sqrt{\frac{D}{T}},\ c_2 = \sqrt{\frac{D}{T}}$, here we have $c_* = \lambda_*(k_0),\ c_1 = v_0 + c(k_0)$, and $c_2 = v_0 - c(k_0)$. Because of $c(k) < 0$, fast waves in the general PW model also reaches vehicles from behind.

There are subtle differences among special cases of the general PW model. In the PW model, where $c(k) = c_0$, the stability condition (34) can be violated and waves grow in magnitude and eventually become shocks in the form of roll waves (Whitham 1974, Kuhne 1984) while in Zhang's model where $c(k) = kv_*^{'}(k)$ the stability condition is always satisfied and waves always damp in magnitude (Zhang 1999). Thus, like the LWR model, Zhang's model is also inherently stable. Moreover, the asymptotic behavior of small perturbations of the kind $k = k_0 + \xi(x,t),\ v = v_0 + w(x,t)$ near equilibrium point (k_0, v_0) ($v_0 = v_*(k_0)$ and ξ, w are small perturbations) in the PW and Zhang models also differ. Such perturbations to Zhang's model can be accurately approximated by a convection equation

$$\xi_t + \lambda_*(k_0)\xi_x = 0, \tag{35}$$

while those to the PW model can be accurately approximated by a diffusion equation

$$\xi_t + \lambda_*(k_0)\xi_x = D_*\xi_{xx}, \quad \text{or} \tag{36}$$

$$\xi_{t'} = D_*\xi_{x'x'} \tag{37}$$

if a moving coordinate $x^{'} = x - \lambda_*(k_0)t,\ t^{'} = t$ is used, where D_* is the diffusion coefficient, and is given by $-(\lambda_1(k_0, v_0) - \lambda_*(k_0))(\lambda_2(k_0, v_0) - \lambda_*(k_0))$, a positive constant (Whitham 1974, del Castillo et al. 1994, and Zhang 1999). Driven by relaxation, any non-equilibrium state (k, v) in the PW model will become closer and closer to its corresponding equilibrium state $(k, v_*(k))$ with the increase of time. This latter behavior, together with the properties of Eq. 37 (i.e., its solutions are smooth), implies that at the end of a queue the PW model does backward smoothing to a sharp density/speed profile, thus predicting possibly negative travel speeds (Daganzo 1995a). Zhang's model, however, is absent of this problem because its solutions are not diffusive.

3.2 Propagation of shock and expansion waves

When traffic conditions undergo sharp transitions, shocks or expansion waves arise. The LWR theory possesses both types of waves and whether a particular kind of wave arises is determined by the entropy condition. A LWR shocks has zero width and travels at a particular speed given by

the Rankine-Hugoniot condition $s = [f_*]/[k]$, which is derived from the integral conservation law. The general PW model also has similar properties. It has both kinds of waves, actually two for each kind—one associated with the first characteristic and the other with the second characteristic. The first is referred to as 1-shock or 1-rarefaction waves, and the second 2-shock or 2- rarefaction waves. Whether a shock or expansion wave arises in a general PW solution is also dependent on entropy conditions, and they are as follows (Zhang 2000a):

$$\text{1-Shock, (E-H1):} \quad \lambda_1(U_r) < s < \lambda_1(U_l),\ s < \lambda_2(U_r), \tag{38}$$

$$\text{2-Shock, (E-H2):} \quad \lambda_2(U_r) < s < \lambda_2(U_l),\ s > \lambda_1(U_l), \tag{39}$$

$$\text{1-Rarefaction, (E-R1):} \quad \lambda_1(U_l) < \lambda_1(U_r), \tag{40}$$

$$\text{2-Rarefaction, (E-R2):} \quad \lambda_2(U_l) < \lambda_2(U_r), \tag{41}$$

And the speeds of shocks are also given by the Rankine-Hugoniot conditions derived from integral conservation laws. A difficulty arises, however, from the fact that the momentum equation is not a conservation law, it is simply an evolution equation for travel speeds. As a result, we do not have a *unique* corresponding integral conservation law for the momentum equation, that is, there are many different integral conservation forms that lead to the momentum equation. Two such examples are:

$$\begin{aligned} \frac{\partial}{\partial t}\int_{x_1}^{x_2} v(x,t)dx &= \left(\frac{v^2}{2}+\phi(k)\right)(x_1,t) - \left(\frac{v^2}{2}+\phi(k)\right)(x_2,t) \\ &+ \int_{x_1}^{x_2} \frac{v_* - v}{\tau}dx, \quad \phi^{'}(k) = \frac{c^2(k)}{k}, \end{aligned} \tag{42}$$

$$\begin{aligned} \frac{\partial}{\partial t}\int_{x_1}^{x_2} (kv)(x,t)dx &= \left(\frac{(kv)^2}{k}+\psi(k)\right)(x_1,t) - \left(\frac{(kv)^2}{k}+\psi(k)\right)(x_2,t) \\ &+ \int_{x_1}^{x_2} \frac{kv_* - kv}{\tau}dx, \quad \psi^{'}(k) = c^2(k). \end{aligned} \tag{43}$$

We cannot tell, from physical principles, which integral form is "correct". The selection of a particular integral form should therefore be guided by field observations, i.e., choosing the one that produces closest shock speeds to field measurements. For illustration purposes, we shall take the simplest, i.e., the first integral form in our subsequent presentations. The same arguments can be applied directly to other integral forms. The first integral momentum equation leads to following *conservative differential form*:

$$v_t + \left(\frac{v^2}{2}+\phi(k)\right)_x = \frac{v_* - v}{\tau}.$$

together with the conservation of mass

$$k_t + (kv)_x = 0,$$

we obtain the system of "conservation " laws with a source term:

$$U_t + F(U)_x = R(U), \tag{44}$$

where $F(U) = \left(kv, \frac{v^2}{2} + \phi(k)\right)^t$, and U, R are as defined before.

The shock speeds of the general PW model is not affected by the presence of the source term, and is still given by the Rankine-Hugoniot condition:

$$s[U] = [F(U)], \tag{45}$$

or

$$s[k] = [kv],\ s[v] = \left[\frac{v^2}{2} + \phi(k)\right].$$

These equations imply a certain relation between k and v. This relation leads to the shock curves (1-shock & 2-shock) in the $k - v$ phase plane (Zhang 2000a).

Expansion (or rarefaction) waves of the general PW model, however, are influenced by the relaxation source term. The strength of this influence is determined by the relaxation time. In a short time (compared to the relaxation time), one can neglect the effect of the source term and obtain certain relations between k, v in an expansion wave solution. These are the 1-rarefaction and 2-rarefaction curves in the $k - v$ phase plane (Zhang 2000a). Over time, however, the cumulative effects of the source term, relaxation, build up into rarefaction wave solutions, and one addresses this problem by modifying the solutions obtained without the source term. Also because of relaxation, the general PW model either approaches to the LWR model or a viscous LWR model $k_t + (kv_*)_x = D_* k_{xx}$, depending on the choice of $c(k)$.

Clearly one cannot ignore the effects of relaxation. Nevertheless, the study of the general PW model without relaxation

$$U_t + F(U)_x = 0 \tag{46}$$

reveals much information about the properties of the general PW model with relaxation. And computations of numerical solutions to the general PW model often rely on the Riemann solutions of (46). Therefore we provide here the solutions of Riemann problems to the general PW model without relaxation (46) (see Zhang 2000a for details).

The solution to the Riemann problem

$$U_t + F(U)_x = 0, \tag{47}$$

$$U(x, t=0) = \begin{cases} U_l, & x < 0 \\ U_r, & x > 0 \end{cases} \tag{48}$$

are of 8 kinds:

1. 1-shock:

$$\text{H1: } v_r - v_l = -\sqrt{\frac{2(k_l - k_r)(\phi(k_l) - \phi(k_r))}{k_l + k_r}},\ k_l < k_r. \tag{49}$$

2. 2-shock:

$$\text{H2: } v_r - v_l = -\sqrt{\frac{2(k_l - k_r)(\phi(k_l) - \phi(k_r))}{k_l + k_r}},\ k_l > k_r. \tag{50}$$

3. 1-rarefaction:

$$\text{R1: } v_r = \int_{k_l} \frac{c(k)}{k} dk,\ k_l > k_r \tag{51}$$

4. 2-rarefaction:

$$\text{R2: } v_r = \int_{k_l} \frac{c(k)}{k} dk,\ k_l < k_r \tag{52}$$

5. 1-shock + 2-shock:

$$\text{H1: } v_m - v_l = -\sqrt{\frac{2(k_l - k_m)(\phi(k_l) - \phi(k_m))}{k_l + k_m}},\ k_l < k_m. \tag{53}$$

$$\text{H2: } v_r - v_m = -\sqrt{\frac{2(k_m - k_r)(\phi(k_m) - \phi(k_r))}{k_m + k_r}},\ k_m > k_r. \tag{54}$$

6. 1-rarefaction + 2-rarefaction:

$$\text{R1: } v_m = \int_{k_l} \frac{c(k)}{k} dk,\ k_l > k_m \tag{55}$$

$$\text{R2: } v_r = \int_{k_m} \frac{c(k)}{k} dk,\ k_m < k_r \tag{56}$$

7: 1-rarefaction + 2-shock:

$$\text{H1: } v_m - v_l = -\sqrt{\frac{2(k_l - k_m)(\phi(k_l) - \phi(k_m))}{k_l + k_m}},\ k_l < k_m. \tag{57}$$

$$\text{H2: } v_r - v_m = -\sqrt{\frac{2(k_m - k_r)(\phi(k_m) - \phi(k_r))}{k_m + k_r}},\ k_m > k_r. \tag{58}$$

8: 1-shock + 2-rarefaction:

$$\text{H1: } v_m - v_l = -\sqrt{\frac{2(k_l - k_m)(\phi(k_l) - \phi(k_m))}{k_l + k_m}},\ k_l < k_m. \tag{59}$$

$$\text{R2: } v_r = \int_{k_m} \frac{c(k)}{k} dk,\ k_m < k_r \tag{60}$$

where $U_m = (k_m, v_m)^t$ is an intermediate state that provides the transition from a 1-wave to a 2-wave.

The transitions are most clearly seen from the phase diagram (Fig. 5). Note that for a state U_l, there are four special curves (H1, R1, H2, R2) emanating from that point, dividing the quarter plane of $k - v$ into four regions: I, II, III, IV. If the downstream U_r in the Riemann problem falls in region I, the solution would be of Type 6 (R1+ R2); in region II, Type 7 (R1+ H2), in region III, Type 5 (H1+H2), and in region IV, Type 8 (H1 + R2). Because of the entropy conditions, the intermediate states always fall on a 1-wave curve (i.e., R1, H1). When U_r falls on a particular wave curve, then the transition involves only one kind of wave and no intermediate state is produced. These are the types 1-4 solutions.

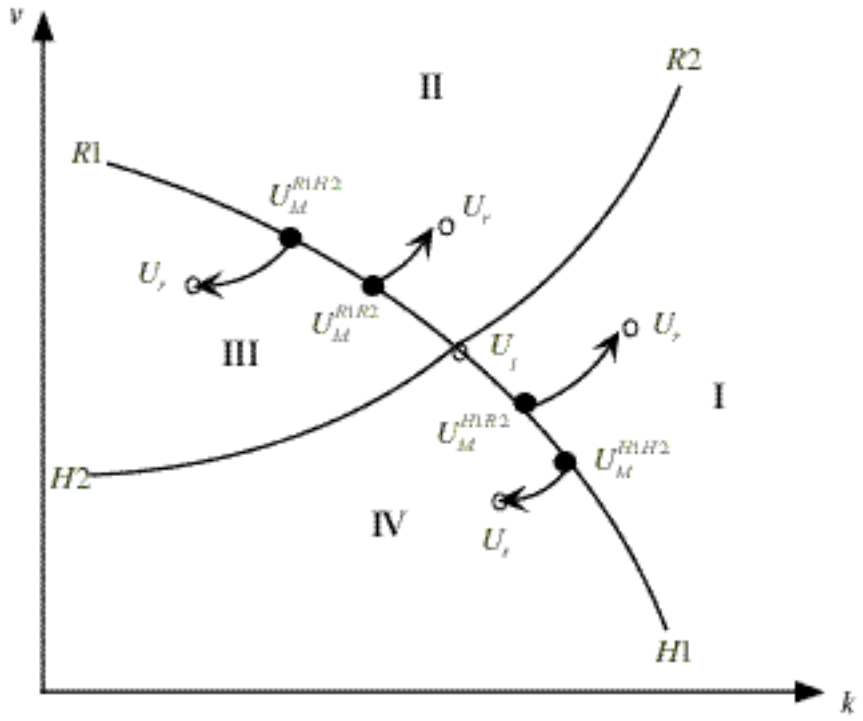

Figure 5: Phase transition diagram in the solution of Riemann problems (adopted from Zhang (2000a))

3.3 Traveling waves, instability and roll waves

Besides traffic sound waves, shock waves and expansion waves, there is another kind of waves in the general PW theory. This is the so-called traveling waves (Whitham 1974, Zhang 1999). It is a wave that has a smooth profile and travels at a constant speed, and takes the following form: $(k, v)(x, t) = (k, v)(\chi),\ \chi = x - st$ (Fig. 7(a)). For the traveling wave solution to arise, a certain stability condition has to be met. When this condition is violated, another kind of waves, the roll waves, may arise. A roll wave is a series of smooth, monotonic profiles separated by jumps (Fig. 6). The existence of roll waves is a direct consequence of traffic instability.

In this section we first obtain the traveling waves, then construct roll waves based on the traveling wave solution. Recall that a traveling wave is a steady profile with a translation speed s:

$$(k, v)(x, t) = (k, v)(\chi),\ \chi = x - st. \tag{61}$$

Substitute the traveling wave solution (61) into the general PW model, one obtains

$$-sk_\chi + (kv)_\chi = 0, \tag{62}$$

$$-sv_\chi + vv_\chi + \frac{c^2(k)}{k}k_\chi = \frac{v_* - v}{\tau}, \tag{63}$$

which after integration and further substitution of terms become

$$\left(c^2(k) - \frac{Q^2}{k^2}\right) k_\chi = f_*(k) - Q - ks, \tag{64}$$

where Q is an integration constant and

$$Q = k(v - s). \tag{65}$$

Because the two states at $x = \pm\infty$, $(k, v) = (k_{1,2}, v_{1,2})$ both satisfy (65), one can compute the speed of the traveling wave

$$s = \frac{k_1 v_1 - k_2 v_2}{k_1 - k_2},$$

which is the same as the shock speed given by the Rankine-Hugonoit condition.

Let $h(k)$ denote the right hand side of (64), then $h^{"}(k) = f^{"}(k) < 0$. Moreover, $h(k)$ crosses the $k-$axis at most twice at $k_a,\ k_b,\ k_a \leq k_b$. These crossing points corresponding to equilibrium concentration values and in between them $h(k) > 0$ (Zhang 1999). Since both $(k, v) = (k_{1,2}, v_{1,2})$ are equilibrium points, $k_{1,2}$ are also roots of $h(k)$. Moreover, we have $k_1 < k_2$, or $k_\chi > 0$ from the fact that $f_*(k)$ is strictly concave. Thus, for a smooth profile of $k(\chi)$ to exist, we must have

$$c^2(k) - \frac{Q^2}{k^2} > 0,$$

which yields the following stability condition

$$v + c(k) < s < v - c(k). \tag{66}$$

That is, the traveling wave must travel slower than the fast characteristic and faster than the slow characteristic.

When the stability condition is met, the smooth traveling wave profile can be obtained by integrating

$$\frac{d\chi}{dk} = \frac{c^2(k) - \frac{Q^2}{k^2}}{f_*(k) - Q - ks}, \tag{67}$$

which is given by:

$$\chi = \int^k \frac{c^2(\eta) - \frac{Q^2}{\eta^2}}{f_*(\eta) - Q - \eta s} d\eta. \tag{68}$$

When the stability condition (66) is violated, that is, the traveling wave travels either faster than the fast characteristic or slower than the slow characteristic, a smooth profile connecting k_1 and k_2 is no longer possible and a discontinuity (i.e., shock) must be inserted at the location where the wave turns back on itself. This time one still obtains a monotonic profile but with a shock separates two smooth pieces (Fig. 7(b)), and the speed of the shock is determined by the R-H shock condition.

There is a special case when the stability condition is not met. This is the case where both the numerator and denominator of (67) vanishes, which leads to non-smooth and periodic solutions to

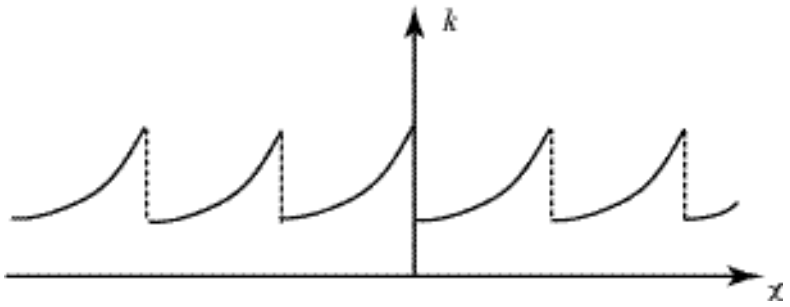

Figure 6: Roll waves in the moving coordinate χ

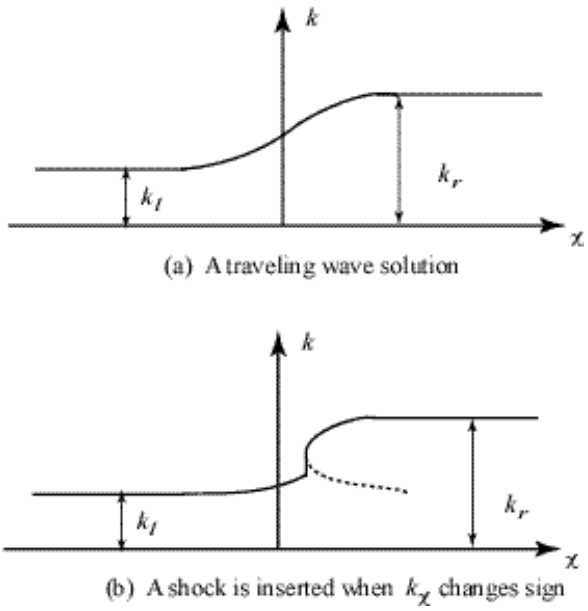

Figure 7: Traveling waves and shocks in the PW model

the general PW model, often referred to as *roll waves* in hydraulic literature. Note that the physical solution of these two algebraic equations is $Q = -k_0 c(k_0)$, where Q is the constant flux measured relative to the moving coordinate χ and k_0 is the critical density that makes both the numerator and denominator of (67) vanish. It is necessary that (k_0, v_0) is an equilibrium state, which fixes the shock speed $s = v_*(k_0) + c(k_0)$. The critical state also fixes the integration constant in the profile equation (68). The roll waves can then be constructed, in the same manner as shown in Dressler (1949), by piecing together the smooth profiles with shocks at appropriate locations, which in turn are determined by the R-H shock conditions. Although the existence of roll wave solutions in the PW model were known to transportation researchers not long after the development of the PW model (e.g., Leutzbach 1985), no one to date has obtained specific roll wave solutions to compare with real world observations of stop-start waves. With the development of Section 3.2, however, this can now be done.

3.4 Summary and Discussions

The PW-like higher-order traffic flow models extend the basic kinematic wave traffic flow model in two ways: they allow for non-equilibrium phase transitions and introduce instability. These are achieved through the addition of a momentum equation that describes speed evolution. The resulting flow obtained from these higher-order models, however, are not all that different than those obtained from the basic kinematic wave model—shocks, for example, exist in both types of models. Moreover, owning to relaxation, similar types of solutions (e.g. shocks or expansion waves) of these two families of models become much similar in long time (typically 10τ).

On the other hand, some significant differences also exist between the two family of models. For one, higher-order models have two family of characteristics and waves as compared to one family of the kinematic wave model. While the first family of waves in the higher-order models behave much like those in the kinematic wave model, the second family behaves quite differently—they travel faster than traffic, and reaches vehicles from behind. This property of the second characteristic has led to doubts about the validity of higher-order traffic models and interesting discussions over the pros and cons of higher-order approximations of traffic flow in general (e.g., Daganzo 1995a, Papageorgiou 1998, Lebacque 1999, Zhang 2001). Because following vehicles usually cannot force leading ones to speed up or slow down. fast-than-traffic waves are quite unrealistic when traffic is on a single-lane highway. When traffic is flowing on a multi-lane highway and passing is allowed, such faster-than-traffic waves do arise as a result of 1) lane-changing, or 2) averaging, or both (see Zhang 2000c for details). Another difference between the two types of models is that higher-order models contain traveling wave and roll wave solutions while the KW model does not. Roll wave solutions are particularly interesting because of their similarity to observed stop-start waves.

Like the kinematic wave model, higher-order models can also be extended to model inhomogeneous roads. This is particularly straightforward with the PW model— one simply replace the homogeneous equilibrium speed-density relation $v_*(k)$ with a space-dependent one $v_*(k, x)$. The extension of higher-order models to model road networks, however, is not as straightforward and is

a worthwhile research topic for traffic flow researchers.

One of the motivations for developing the PW model was to remove shocks from the model solutions. This, however, is not fulfilled by the higher-order models that we have covered up to now, although the PW model does admit smooth traveling wave solutions. Higher-order space derivatives, in the form of k_{xx} or v_{xx} must be introduced to obtain shocks with a structure. We call these models diffusive or viscous (higher-order) models. In contrast, PW like models are called inviscid higher-order models. The next section briefly introduces some of the popular viscous traffic models, and a stochastic extension to a particular viscous higher-order model.

4 Diffusive, viscous and stochastic traffic flow models

4.1 Diffusive and viscous traffic flow models

The first diffusive traffic flow model, which was mentioned in the classical book of Whitham (1974) was obtained by considering a flux that is dependent not only on vehicle concentration, but also on the concentration gradient:

$$q = f_*(k) - \nu k_x,$$

which, after substitution into the conservation equation, leads to

$$k_t + f_*(k)_x = \nu k_{xx}, \tag{69}$$

where ν is a positive parameter.

This diffusive model, when $f_*(k)$ is quadratic, can be manipulated into the following form

$$c_t + cc_x = \nu c_{xx}, \quad c = f_*^{'}(k), \tag{70}$$

which is the well-known Burger's equation.

Analytical solutions to the Burger's equation with given initial data can be obtained through the so-called Cole-Hopf transformation. We refer the reader to Whitham (1974, pp 96-112) for the detailed solution formulas and only discuss the qualitative properties of various kinds of solutions to the Burger's equation. These are:

1. The solution to the initial value problem $c_t + cc_x = \nu c_{xx},\ c(x, t = 0) = F(x)$ always exists, and is smooth after $t > 0$.

2. When $\nu \to 0$, the solution approaches that of $c_t + cc_x = 0$.

3. For initial data $F(x) = \begin{cases} c_l & x < 0 \\ c_r & x > 0, \end{cases}$ $c_l > c_r$ (A step function), the solution is a traveling wave $c(x - st)$, with $s = \frac{c_1+c_2}{2}$. The width of the traveling wave, as measured by the range where 90% of the change in $c_l - c_r$ occurs, is proportional to $\frac{\nu}{c_l - c_r}$. As $\nu \to 0$, the width of the traveling wave becomes nil and the traveling wave becomes a shock of $c_t + cc_x = 0$. Thus the viscous model provides a shock structure to the LWR model.

4. For initial data $F(x) = A\delta(x)$ (A single hump), the solution is a nonlinear diffusion wave, similar to those of the heat equation $c_t = \nu c_{xx}$ when $R = \frac{A}{2\nu} \ll 1$.

5. Also, N-waves and periodic waves can be found in the solution with proper initial data.

Clearly, the addition of the second order derivative k_{xx} to the LWR conservation law does two things to it because of diffusion: 1) it smoothes the shocks of the LWR conservation law, thereby providing a shock structure, and 2) it guarantees the uniqueness of solution for small ν, thereby providing a way to pick solutions from the LWR conservation law. This latter property is often exploited in numerical computations of shock wave solutions.

The diffusion corrected conservation law of (69), when $f_*(k)$ is not quadratic, can be approximated by the Burger's equation. In fact, the aforementioned properties of the Burger's equation (except Property #2, which must be modified) are shared by all known diffusion corrected or viscous traffic flow models, including the following popular viscosity-corrected PW model:

$$\begin{pmatrix} k \\ v \end{pmatrix}_t + \begin{pmatrix} v & k \\ \frac{c^2(k)}{k} & v \end{pmatrix} \begin{pmatrix} k \\ v \end{pmatrix}_x = \begin{pmatrix} 0 \\ \frac{v_*-v}{\tau} \end{pmatrix} + \begin{pmatrix} 0 & 0 \\ 0 & \nu \end{pmatrix} \begin{pmatrix} k \\ v \end{pmatrix}_{xx}. \tag{71}$$

The viscosity-corrected PW model, however, can become unstable in certain ranges of traffic and therefore has additional properties. These properties, including the collapse of homogeneous traffic under local and global perturbations and the formation of vehicle-clusters in stop-and-go traffic, are well documented in (Kerner &Konhaüser 1993, 1994; Kerner, Konhaüser & Schilke 1995; Kerner and Rehborn 1999; Kühne & Beckschulte 1993). Interested readers are referred to the aforementioned literature for detailed discussions of these properties.

4.2 Acceleration noise and a stochastic flow model

Same as section 5.3 in the original text.

5 Numerical approximations of continuum models

All of our continuum models are described by partial differential equations, some (i.e, LWR, PW and Zhang) are hyperbolic while others (e.g., the viscous model of (69)) parabolic. Proper initial/boundary conditions must be prescribed to these equations to form a well posed problem. The solutions of continuum models involving general initial/boundary conditions are tedious, if not difficult, to obtain analytically. Numerical procedures are often employed to solve such problems.

Typically, finite difference methods are applied to solve hyperbolic traffic flow models while finite difference or finite element methods are used to solve parabolic traffic flow models. Both methods start with a discretization of the time-space domain ($t \geq 0, -L < x < L$), with the following grid mesh being the most common:

$$\begin{aligned} x_i &= ih, \quad i = 0, \pm 1, \pm 2, \cdots, L/h, \\ t_j &= jk, \quad j = 0, \ \ 1, \ \ 2, \ \cdots, T/k. \end{aligned}$$

where $h \equiv \Delta x$ and $k \equiv \Delta t$, and (x_i, t_j) are the grid points of this mesh.

Let the values of $U(x,t)$ on those grid points denoted by U_i^j (see Fig. 8). Then the time-space derivatives in a continuum model can be approximated using values at these grid points, and we obtain a set of finite difference equation(s) (FDE). For example, the space derivative U_x can be approximated in a number of ways:

$$[U_x]_i^j = \begin{cases} \frac{U_i^j - U_{i-1}^j}{h}, & \text{Forward Difference} \\ \frac{U_{i+1}^j - U_{i-1}^j}{2h}, & \text{Center Difference} \\ \frac{U_{i+1}^j - U_i^j}{h}, & \text{Backward Difference} \end{cases} \tag{72}$$

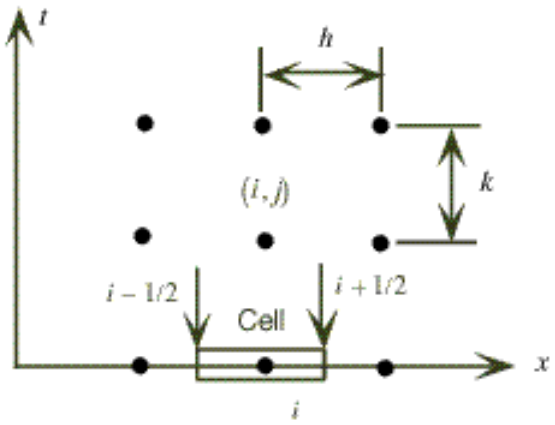

Figure 8: Time-space grid

However, the numerical approximation of continuum models is not a simple exercise of replacing continuous variables and their derivatives with discrete ones and their differences. This is particularly true for hyperbolic traffic models, because in these models discontinuities or shock waves can develop spontaneously even from smooth initial data. The existence of shocks presents a major challenge to the development of numerical approximations that are *consistent* with and *convergent* to the model equations when the mesh size is further and further refined. A valid approximation must meet the following three conditions:

1. it is consistent with the original PDE, i.e., the FDE converges to the PDE when h and κ approach 0 (*consistency*),

2. numerical errors introduced by the FDE do not increase over time (*stability*), and

3. its solutions converge to the right solutions of the original PDE when h and κ approach 0 (*convergence*).

In this section we present two consistent, stable and convergent finite difference approximations of the system (31) with initial/boundary data of (73) and a finite element approximation of the

viscous model (33) with the same initial and boundary data. It should noted that the LWR, PW and Zhang models can all be expressed in the form of (31). Therefore the finite difference approximations presented here applies to all three models. We begin our presentation with finite difference approximations.

5.1 Finite difference methods for solving inviscid models

In this section we present two finite difference schemes to solve the system of (31) with the following initial/boundary data:

$$\begin{aligned} &\text{I.C.:} \quad U(x,0) = U_0(x),\ -L \le x \le L \\ &\text{B.C.:} \quad U(-L,t) = U_-(t),\ U(L,t) = U_+(t),\ t \ge 0. \end{aligned} \tag{73}$$

where U_0 and $U_\pm$ are vector valued functions of space and time, respectively, and may contain a countable number of jumps. This system of equations include the Kinematic wave model of LWR, the higher-order models of Payne-Whitham and of Zhang.

It turns out that a particular form of hyperbolic PDEs, called the conservative form, is specially suited for developing finite difference schemes that ensure the aforementioned three conditions. A conservative form of (31), for example, is given by (44), i.e.,

$$U_t + F(U)_x = R(U).$$

(44) is called a conservative form because it arises from certain conservative phenomena in convective transport:

$$\frac{\partial}{\partial t}\int_L U(x,t)dx + \int_{\partial L} F(U)dx = \int_L R(U)dx. \tag{74}$$

For example, the conservation of vehicles on a finite road segment $[x_1, x_2]$ leads to a specific case of (74):

$$\frac{\partial}{\partial t}\int_{x_1}^{x_2} k(x,t)dx + (kv)(x_2,t) - (kv)(x_1,t) = \int_{x_1}^{x_2} r(k,v)dx. \tag{75}$$

Using the conservative form, we can develop a *conservative finite difference approximation* of (44). The advantage of a conservative finite difference approximation is that it ensures the correct computation of shock speeds. A finite difference approximation of (44) is conservative if it can be written as

$$\frac{U_i^{j+1} - U_i^j}{\kappa} + \frac{\tilde{F}(U_{i+1}^j, U_i^j) - \tilde{F}(U_i^j, U_{i-1}^j)}{h} = \tilde{R}(U_{i+1}^j, U_i^j, U_{i-1}^j), \tag{76}$$

where $\tilde{F}$ in (76) is called *numerical flux* (explained later) [3]. When a finite difference scheme is in conservative form, the condition for consistency is particularly simple. It requires that the numerical flux function satisfies

$$\tilde{F}(U,U) = F(U).$$

[3]The argument list of the numerical flux function can involve more than two nodal points, depending on the required accuracy of the finite difference approximation. (76) uses two nodal values to compute its numerical flux and is first order accurate.

Examples of consistent conservative finite difference schemes in traffic flow are the finite difference schemes of (Michalopoulos, Beskos & Lin (1984)), (Daganzo 1994), and (Lebacque, 1996) in the scalar case (i.e., the LWR model), the finite difference scheme of Leo and Pretty (Leo and Pretty 1992) and Zhang (2000b) in the system case (e.g., the PW model).

A consistent, conservative finite difference approximation, if linear, is guaranteed to converge to the correct solution if it meets a stability condition (LeVeque 1992). This condition, generally referred to as the CFL (Courant-Friedrichs-Lewy) condition, says that the cell advance speed $\frac{h}{\kappa}$ cannot be greater than the maximum absolute characteristic velocity, i.e.,

$$\max \left| \frac{\kappa}{h} \lambda_i \right| \leq 1, \ i = 1, \cdots, n.$$

Although this theorem has not been proven for most nonlinear systems, computational experiences indicate that the CFL condition is sufficient to ensure convergence for a large number of nonlinear systems. Thus we require the CFL condition in all of our finite difference approximations.

The remaining task in our finite difference approximations is to obtain the numerical flux function that ensures the consistency, stability and convergence properties. Before explaining what a numerical flux function is, we first make clear what U_i^j represents in our scheme of things. Suppose that $u(x,t)$ is a weak solution of the integral conservation law (74). We can write (74) as

$$\begin{aligned} \int_{x_{i-1/2}}^{x_{i+1/2}} u(x,t_{j+1})dx &= \int_{x_{i-1/2}}^{x_{i+1/2}} u(x,t_j)dx + \int_{t_j}^{t_{j+1}} \int_{x_{i-1/2}}^{x_{i+1/2}} R(u(x,t))dxdt \\ &- \left[\int_{t_j}^{t_{j+1}} F(u(x_{i+1/2},t)dt - \int_{t_j}^{t_{j+1}} F(u(x_{i-1/2},t)dt \right] \end{aligned} \tag{77}$$

where $i-1/2$ and $i+1/2$ denotes the left and right boundary of cell i (see Fig. 8), respectively. If we interpret U_i^j as the cell average

$$U_i^j = \frac{1}{h} \int_{x_{i-1/2}}^{x_{i+1/2}} u(x,t_j)dx \tag{79}$$

then

$$\tilde{F}(U_{i+1}^j, U_i^j) = \frac{1}{\kappa} \int_{t_j}^{t_{j+1}} F(u(x_{i+1/2},t)dt \tag{80}$$

is the average flux passing through the cell boundary $x_{i+1/2}$ in the time interval (t_j, t_{j+1}), and

$$h\tilde{R} = \frac{1}{\kappa} \int_{t_j}^{t_{j+1}} \int_{x_{i-1/2}}^{x_{i+1/2}} R(u(x,t))dxdt$$

is the average inflow into cell i from the source during time interval (t_j, t_{j+1}). With these definitions, the integral conservation law (74) reduces to (76), and this is why (76) is called a conservative approximation.

There are a number of ways to construct a numerical flux function, perhaps the most intuitive and illustrative is the one obtained using Godunov's finite difference method. The Godunov method solves locally a Riemann problem at each cell boundary for the time interval (t_j, t_{j+1}), using the

cell averages U_i^j as initial data. It then pieces together these Riemann solutions at time t_{j+1} and average them using (79) to obtain new initial data for t_{j+2}, and this process is repeated until T/k is reached. Recall that the Riemann problem for the homogeneous equation

$$U_t + F(U)_x = 0 \tag{81}$$

of our continuum traffic models have been solved in Sections 2 and 3. We can then apply the principle of superposition to solve the traffic models with source terms:

$$U_t + F(U)_x = R(U). \tag{82}$$

Using the aforementioned procedure, we obtain a Godunov type of difference equation for (44):

$$\frac{U_i^{j+1} - U_i^j}{k} + \frac{F\left(U_{i+1/2}^{*j}\right) - F\left(U_{i-1/2}^{*j}\right)}{h} = \tilde{R}. \tag{83}$$

in which the numerical flux function reads

$$\tilde{F}(U_{i+1}^j, U_i^j) = F\left(U_{i+1/2}^{*j}\right), \tag{84}$$

and the source flux is computed by

$$\tilde{R} = R\left(\frac{U_{i+1} + U_{i-1}}{2}\right).$$

The variables $U_{i+1/2}^{*j}, i = 0, \pm 1, \pm 2, \cdots, \pm L/h$ are obtained from solving a series of Riemann problems to the homogeneous equation at cell boundaries. Owing to space limitations, we cannot in this monograph fully describe how this is done for higher-order models (interested readers are referred to Zhang 2000b). However, the computation of $U_{i+1/2}^{*j}$ is particularly simple when the equilibrium relation $v = v_*(k)$ is assumed. It leads to the following finite difference equation

$$\frac{k_i^{j+1} - k_i^j}{k} + \frac{f_*\left(k_{i+1/2}^{*j}\right) - f_*\left(k_{i-1/2}^{*j}\right)}{h} = 0,\ v_i^{j+1} = v_*(k_i^{j+1}), \tag{85}$$

where the cell boundary flow $f_*\left(k_{i+1/2}^{*j}\right)$ is given by a simple formula (LeVeque 1992, Bui, et. al. 1992):

$$f_*\left(\rho_{i+1/2}^{*j}\right) = \begin{cases} \min_{k_i^j \le k \le \rho_{i+1}^j} f_*(k), & \text{if } k_i^j < k_{i+1}^j \\ \max_{k_i^j \ge k \ge \rho_{i+1}^j} f_*(k), & \text{if } k_i^j > k_{i+1}^j \end{cases}.$$

When $f_*(k)$ is concave, this formula can be further streamlined through the introduction of a supply and demand function for each cell (Daganzo 1994, 1995b; Lebacque 1996):

$$\text{Demand: } D(i,j) = \begin{cases} f_*(k_i^j), & \text{if } \frac{j}{i} < k* \\ f(k^*), & \text{if } \frac{j}{i} \ge k* \end{cases}, \tag{86}$$

$$\text{Supply: } S(i,j) = \begin{cases} f_*(k_i^j), & \text{if } k_i^j > k* \\ f(k^*), & \text{if } k_i^j \le k* \end{cases}, \tag{87}$$

where k^* is the critical density at which $f_*^{'}(k^*) = 0$. And we have

$$f_* \left(k_{i+1/2}^{*j} \right) = \min\{D_i, S_{i+1}\}, \tag{88}$$

which also applies to boundary cells and bottlenecks.

Another difference approximation of (31) uses the idea of Lax-Friedrichs center differencing. It leads to the following numerical flux:

$$\tilde{F}(U_{i+1}^j, U_i^j) = \frac{F(U_{i+1}^j) + F(U_i^j)}{2} - \frac{h}{\kappa} \frac{U_{i+1}^j + U_i^j}{2}. \tag{89}$$

It is easy to check that this flux function meets the consistency requirement and the resulting finite difference approximation

$$U_i^{j+1} = \frac{U_{i+1}^j + U_i^j}{2} - \frac{\kappa}{2h} \left[F(U_{i+1}^j) - F(U_{i-1}^j) \right] + h\kappa\tilde{R}$$

is also conservative. This center difference scheme remained till recent years a popular choice of approximation of the kinematic wave model (e.g., Michalopolous 1988, Michalopolous, Beskos & Yamauchi 1984, Michalopolous, Kwon, & Khang 1991, Michalopolous, Lin, & Beskos 1987) and being used lately to approximate higher-order models (Zhang 2000d). Zhang and Wu (1999) investigated the convergence properties of this scheme and found that in comparison with Godunov-type of schemes, the center difference scheme has faster convergence rate with respect to expansion wave solutions and slower convergence rate with respect to shock solutions. The reason is that this difference scheme has built-in numerical viscosity which smoothes shocks.

5.2 Finite element methods for solving viscous models

Apart from finite difference methods, the method of finite element is also employed to solve continuum traffic flow equations. In this section we show how the latter is used to solve the viscosity-corrected PW equations.

First we introduce an auxiliary variable w : $w = v_x$, and normalize all the state and time-space variables in the following way:

$$k' = \frac{k}{k_{jam}} \qquad v' = \frac{v}{v_f} \qquad w' = \frac{w}{v_f} \qquad x' = \frac{x}{v_f \tau} \qquad t' = \frac{t}{\tau}. \tag{90}$$

Then the unknown variables in the viscosity-corrected PW model can be expressed by a vector

$$\eta = \begin{pmatrix} k' \\ v' \\ w' \end{pmatrix} \tag{91}$$

and the model itself by the following vector-valued quasi-linear partial differential equation:

$$A\eta_t + B\eta_x = C \tag{92}$$

with (note that for convenience the $'$'s are dropped from the notations)

$$A = \begin{pmatrix} 1 & 0 & 0 \\ 0 & 1 & 0 \\ 0 & 0 & 0 \end{pmatrix} \qquad B = \begin{pmatrix} v & 0 & 0 \\ \frac{1}{k}\frac{1}{Fr} & 0 & \frac{1}{R_e} \\ 0 & 1 & 0 \end{pmatrix} \qquad C = \begin{pmatrix} & -kw & \\ -vw & +v_* & -v \\ & w & \end{pmatrix}, \tag{93}$$

$$\begin{aligned} Fr \equiv \text{Froude number} &= \frac{\text{kinetic energy (inertia influence)}}{\text{potential energy(pressure)}} \\ &= \frac{\left(\frac{1}{2}\right) k v_f^2}{c_0^2 k} = \left(\frac{v_f}{c_0}\right)^2 \\ R \equiv \text{Reynolds number} &= \frac{\text{length velocity}}{\text{kinem. viscosity}} = \frac{v_f^2 \tau}{\nu_0}. \end{aligned} \tag{94}$$

The problem also comes with possibly two initial conditions and six boundary conditions. Because of the hyperbolic nature of the viscosity-corrected PW model, however, only certain combinations of these initial/boundary data are allowed.

In the finite element method, we replace the continuous functions

$$\eta(x,t) = \begin{pmatrix} k(x,t) \\ u(x,t) \\ w(x,t) \end{pmatrix} \tag{95}$$

by functions defined as a lattice:

$$\eta(x_0 + i\Delta x, t_0 + j\Delta t) \equiv \eta_{i,j} \tag{96}$$

and all derivatives by center difference quotients:

$$\eta_x \to \frac{1}{2\Delta x}(\eta_{i+1,j+1} - \eta_{i,j+1} + \eta_{i+1,j} - \eta_{i,j}) \tag{97}$$

and the function values by the midpoint values:

$$\eta_t \to \frac{1}{2\Delta t}(\eta_{i+1,j+1} + \eta_{i,j+1} - \eta_{i+1,j} - \eta_{i,j}). \tag{98}$$

$$\eta \to \frac{1}{4}(\eta_{i+1,j+1} + \eta_{i,j+1} + \eta_{i+1,j} + \eta_{i,j}) \tag{99}$$

We then do step-wise integration, starting from time step $j = 0$ and ending at time step $j = J$, as shown in Fig. (fig 5.16 from original text). To ensure the stability of the numerical procedure, an implicit integration scheme is used to compute the unknown variables $\eta_{i,j},\ \eta_{i+1,j}$ (for notational simplicity we'll drop subscript j in the remaining text of this section). It turns out that the Newtonian iteration procedure is perfectly suited for this purpose. In this procedure the variables $\eta_i,\ \eta_{i+1}$ are replaced by an approximation $\tilde{\eta}_i,\ \tilde{\eta_{i+1}}$ and the deviations $\delta\eta_i,\ \delta\eta_{i+1}$ are computed by linearizing the original equations. Denoting the deviation vector by

$$\delta_i \equiv \begin{pmatrix} \delta & k_i \\ \delta & u_i \\ \delta & w_i \end{pmatrix} \tag{100}$$

then the basic equations can be written in the form of

$$A_i\delta_{i+1} + B_i\delta_i = R_i \tag{101}$$

with

$$\left(\alpha = \frac{2}{\Delta x}, \beta = \frac{2}{\Delta t}, \kappa = \frac{1}{Fr} = \frac{c_0^2}{v_f^2}\right) \tag{102}$$

$$A_i = \begin{pmatrix} \beta + \alpha U + W & K_x & K \\ -U_e'(K) - \kappa\frac{K_x}{K^2} + \alpha\kappa\frac{1}{K} & \beta + W + 1 & U - \alpha\nu \\ 0 & \alpha & -1 \end{pmatrix} \tag{103}$$

$$B_i = \begin{pmatrix} \beta - \alpha U + W & K_x & K \\ -U_e'(K) - \kappa\frac{K_x}{K^2} - \alpha\kappa\frac{1}{K} & \beta + W + 1 & U + \alpha\nu \\ 0 & \alpha & -1 \end{pmatrix} \tag{104}$$

$$R_i = -4\begin{pmatrix} K_t + K_x U + K \\ U_t + UW - U_e(K) + U + \kappa\frac{K_x}{K} - \nu W_x \\ U_x - W \end{pmatrix} \tag{105}$$

where abbreviations

$$K = \frac{1}{4}(\overline{k}_{i+1} + \overline{k}_i + k_{i+1,j} + k_{i,j}) \tag{106}$$

$$K_t = \frac{1}{2\Delta t}(\overline{k}_{i+1} + \overline{k}_i - k_{i+1,j} - k_{i,j}) \tag{107}$$

are used.

Starting with the initial condition as the lowest approximation

$$\overline{\eta}_i = \eta_{i,j=0} \quad \eta_{i-1} = 0 \tag{108}$$

and using the left boundary condition

$$k_{i=0,j}, V_{i=0,j} \Longrightarrow \delta_0 = \begin{pmatrix} 0 \\ 0 \\ \delta w_0 \end{pmatrix} \tag{109}$$

the δ_i is computed recursively by

$$\delta_{i+1} = A_i^{-1}(R_i - B_i\delta_i) \tag{110}$$

as a function of δw_0, which in turn is determined by the right boundary condition

$$v_{i=I,j} \Longrightarrow \delta_I = \begin{pmatrix} \delta k_I \\ 0 \\ \delta w_I \end{pmatrix}. \tag{111}$$

An alternative rearrangement of the deviations δ_i is possible in order to produce a tridiagonal form which facilitates the fit of the boundary conditions (Kerner and Konhaüser, 1993).

5.3 Applications

5.3.1 Calibration of model parameters with field measurements

All the continuum models discussed in this monograph contain certain static relations and parameters. These relations include, for the LWR model, the fundamental diagram $f_*(k)$, and for higher-order models, $v_*(k)$. Since $f_*(k) = kv_*(k)$, knowing one would know the other. The parameters include, but not limited to, free flow speed v_f, jam wave speed c_j, sound speed $c_0(< 0)$ (PW model), jam density k_{jam}, critical density k_c, capacity q_c, and relaxation time τ (PW model). These relations and parameters capture certain fundamental characteristics of the *local* driving environment and driver population, and have to be calibrated/obtained locally before application of the corresponding models. The attainment of the parameters are achieved in two ways: direct measurement and data fitting. The former, when its cost is acceptable, is always preferred if there's a a choice of the two.

The interpretations of the parameters, in most cases, are straightforward and intuitive, which also suggest ways to measure them directly from field data. Among the various speeds, for example, one can easily measure free flow speed and jam wave speed, but not traffic sound speed c_0. For those parameters that can be directly measured, to obtain them is a simple matter of data gathering and processing and we will not elaborate on them here. Rather, we focus on the calibration of those parameters that have confusing interpretations in literature and are difficult to measure directly. These include sound speed c_0 and relaxation time τ.

Recall that the definition of traffic sound speed is the speed of sound waves minus the speed of traffic that carries these sound waves. In the LWR model, the sound wave speeds are $f_*^{'}(k)$, and the traffic speed is $v_*(k)$, therefore $c_0 = f_*^{'}(k) - v_*(k) = kv_*^{'}(k)$ is variable. That is, sound speed in the LWR (and Zhang's model for that matter) is not a fundamental parameter. The PW model, however, fixes the sound speed c_0 as a fundamental parameter and assumes that it is a constant. The latter assumption is questionable because it is unlikely that drivers respond to stimuli with the same intensity under free-flow and jam traffic conditions. With that being said, we turn our attention to the possible ways of measuring c_0. Recall that $\lambda_{1,2} = v \pm c_0$ in the PW model, which suggests that if we can measure the speed of the slower wave λ_1 and traffic speed v, we can then compute the sound speed c_0. This can be done with instrumented vehicles on a single lane-highway where one can measure the acceleration, speed and position of each vehicle in the traffic stream. Clearly, this is a costly way of obtaining sound speed and is rarely done in practice. In reality, c_0, together with another parameter τ, is obtained through data fitting.

Before describing the data fitting procedure, we want to reexamine the interpretation of τ, such that we have a sense of its range and would know roughly if the value obtained from our data fitting exercise makes sense. Relaxation in traffic flow refers to the process where non-equilibrium traffic approaches equilibrium traffic overtime[4]. The pace of this process is controlled by relaxation time τ. Clearly, τ takes the human reaction time as its lower limit, which is about $1 - 1.8$ seconds. Its

[4]one should not confuse the latter with free-flow traffic, although free-flow traffic is also equilibrium traffic, so is jam traffic!

upper limit, in theory, can be infinite. In practice, one never observes congestion that lasts longer than a day, not to mention infinite. The upper limit of relaxation, one speculates, would be in the order of a few minutes, the period of a stop-start wave. This speculation tends to be supported by existing calibration exercises (del Castillo and Benitez 1995, Cremer et al 1993, Kühne 1991, 1984, Papageorgiou et al 1990) that reported τ values ranging from1.8s to 108s.

The calibration of model parameters through data fitting usually involves the following steps:

1. Data collection: collection of road data in the forms of number of lanes, locations of ramps, and so forth, and traffic data, in the forms of time series data of flux, occupancy and spot speeds, at various locations,

2. Numerical approximations of the traffic flow model involved,

3. Calibration: obtain the fundamental diagram for each location from measured data, which in turn determines parameters such as free-flow speed, jam density, capacity flux, and jam wave speed, and obtain other parameters in the model through data fitting.

The process of data fitting involves minimizing some pre-defined performance measures. One common measure is the sum of square errors between model outputs and measured data:

$$PI = \gamma_1 \int dt \left(v_{cal.}(d,t) - v_{meas.}(d,t)\right)^2 + \gamma_2 \int dt \left(k_{cal.}(d,t) - k_{meas.}(d,t)\right)^2 \tag{112}$$

which is a function of model parameters to be calibrated, e.g.,

$$PI = PI(c_0, \tau) \tag{113}$$

for the PW model.

Because of the hyperbolic nature of the continuum traffic flow models, it is crucial to make sure that the finite difference or finite element approximations are correct and accurate. For this reason it is advocated that another step be added to the calibration or validation procedure: the step of checking the finite difference approximation (Zhang 2001). The best way to check the correctness of a numerical approximation, apart from theoretical considerations, is to run through benchmark problems, such as Riemann problems. In this way one can rid of transient and boundary conditions that may hide the inadequacies of the approximation (Zhang 2001).

For the specific examples of calibrating the model parameters, the readers are referred to the following literature:

- del Castillo and Benitez 1995 (A2 Amsterdam-Utrecht, the Netherlands).
- Kühne and Langbein-Euchner 1993 (A3 Fürth-Erlangen near Nuremberg, Germany)
- Papageorgiou et al 1990 (Boulevard Peripherique, Paris, France), and
- Sailer 1996 (Interstate 35W in Minneapolis, Minnesota, U.S.A.).

5.3.2 Multilane traffic flow dynamics

Numerical examples of a two-lane ring road to be provided by Panos?

5.3.3 Traffic flow on a ring road with a bottleneck[5]

In this section we use the finite difference approximations of the LWR and PW models developed earlier to simulate traffic on a ring road. The length of the ring road is $L = 800l = 22.4$ km. The simulation time is $T = 500\tau = 2500$ s $= 41.7$ min. We partition the road $[0, L]$ into $N = 100$ cells and the time interval $[0, T]$ into $K = 500$ steps. Hence, the length of each cell is $\Delta x = 0.224$ km and the length of each time step is $\Delta t = 5$ s. Since $\lambda_* \leq v_f = 5l/\tau$, we find the CFL condition number

$$\lambda_* \frac{\Delta t}{\Delta x} \quad \leq \quad 0.625 < 1.$$

Moreover, we adopt in this simulation the fundamental diagram used in (Kerner and Konhäuser, 1994; Herrman and Kerner, 1998) with the following parameters: the relaxation time $\tau = 5$ s; the unit length $l = 0.028$ km; the free flow speed $v_f = 5.0l/\tau = 0.028$ km/s $= 100.8$ km/h; the jam density of a single lane $\rho_j = 180$ veh/km/lane; $c_0 = 2.48445l/\tau = 0.014$ km/s $= 50.0865$ km/h; The equilibrium speed-density relationship is therefore

$$v_*(\rho, a(x)) = 5.0461 \left[\left(1 + \exp\{[\frac{\rho}{a(x)\rho_j} - 0.25]/0.06\} \right)^{-1} - 3.72 \times 10^{-6} \right] l/\tau,$$

where $a(x)$ is the number of lanes at location x. The equilibrium functions $v_*(\rho, a(x))$ and $f_*(\rho, a(x))$ are given in **Figure** 9.

The first simulation is about the homogeneous LWR model. Here we assume that the ring road has single lane everywhere; i.e., $a(x) = 1$, for $x \in [0, L]$, and use a global perturbation as the initial condition

$$\begin{array}{rcll} \rho(x,0) & = & \rho_h + \Delta\rho_0 \sin \frac{2\pi x}{L}, & x \in [0, L], \\ v(x,0) & = & v_*(\rho(x,0), 1), & x \in [0, L], \end{array} \tag{114}$$

with $\rho_h = 28$ veh/km and $\Delta\rho_0 = 3$ veh/km; and the corresponding initial condition (114) is depicted in **Figure** 10.

The results are shown as *contour plots* in **Figure** 11, from which we observe that initially wave interactions are strong but gradually the bulge sharpens from behind and expands from front to form a so-called N-wave that travels around the ring with a nearly fixed profile.

In the second simulation we created a bottleneck on the ring road with the following lane configuration:

$$a(x) \quad = \quad \begin{cases} 1, & x \in [320l, 400l), \\ 2, & \text{elsewhere .} \end{cases} \tag{115}$$

[5]The results in this section are from unpublished material of Jin and Zhang (2000a,b)

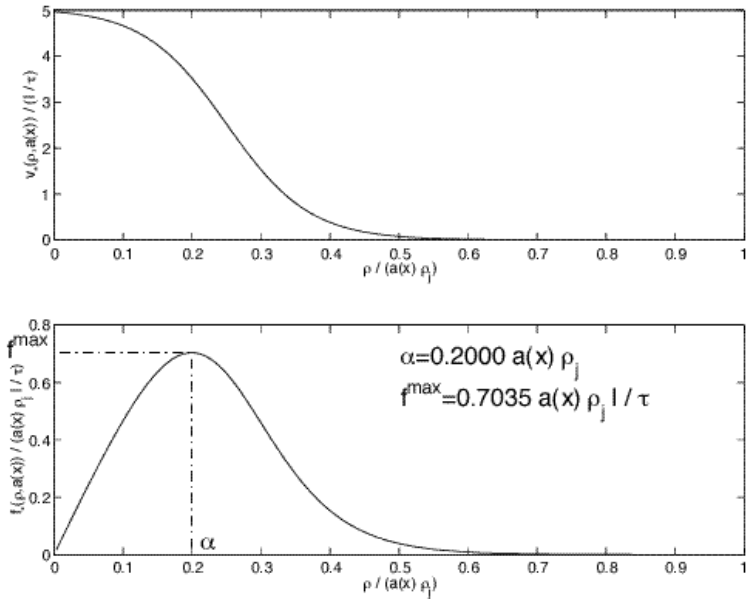

Figure 9: The Kerner-Konhäuser model of speed-density and flow-density relations

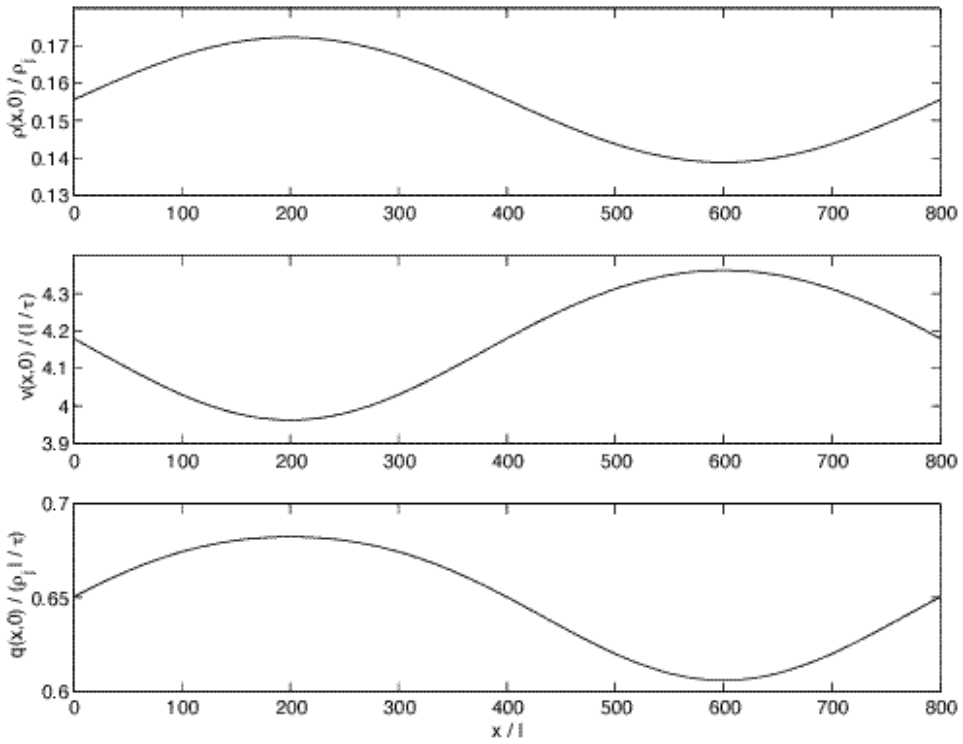

Figure 10: Initial condition (114) with $\rho_h = 28$ veh/km and $\Delta\rho_0 = 3$ veh/km

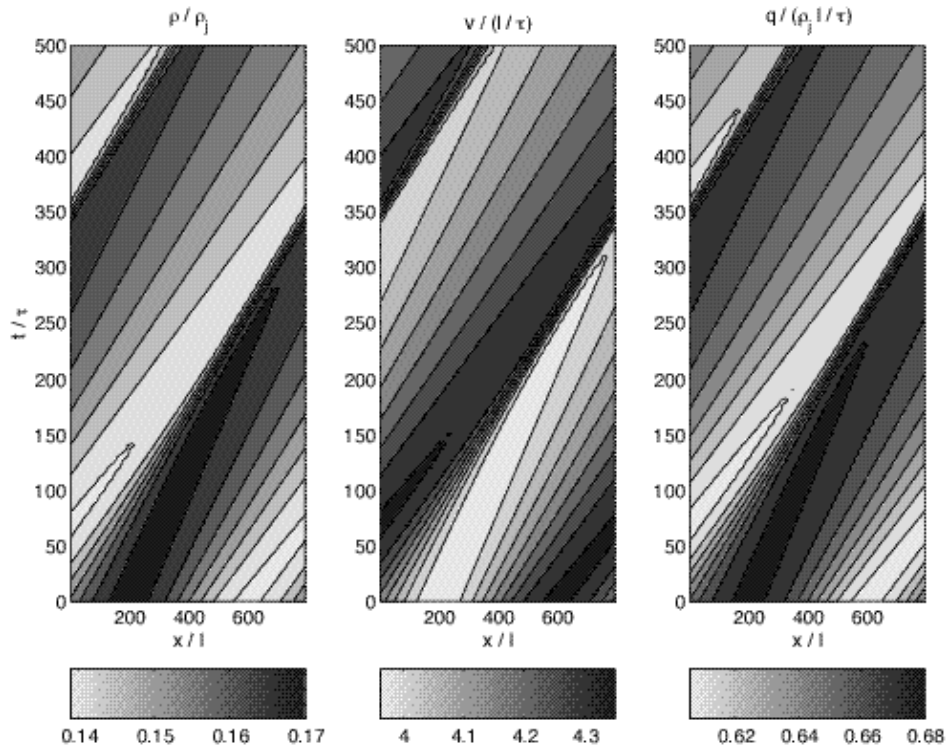

Figure 11: Solutions of the homogeneous LWR model with initial condition in **Figure** 10

As before, we also use a global perturbation as the initial condition

$$\begin{aligned} \rho(x,0) &= a(x)(\rho_h + \Delta\rho_0 \sin \tfrac{2\pi x}{L}), \quad x \in [0,L], \\ v(x,0) &= v_*(\rho(x,0), a(x)), \qquad\qquad x \in [0,L], \end{aligned} \tag{116}$$

with $\rho_h = 28$ veh/km/lane and $\Delta\rho_0 = 3$ veh/km/lane (the corresponding initial condition (116) is depicted in **Figure** 12).

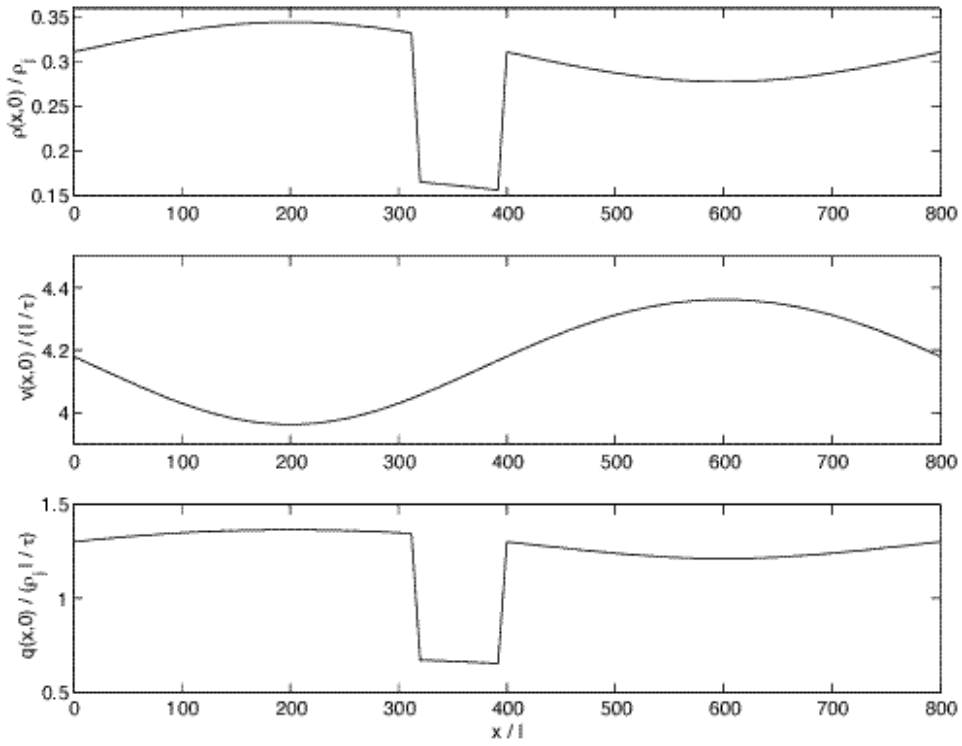

Figure 12: Initial condition (116) with $\rho_h = 28$ veh/km/lane and $\Delta\rho_0 = 3$ veh/km/lane

The results for this simulation are shown in **Figure** 13, and are more interesting. We observe from this figure that at first flow increases in the bottleneck to make the bottleneck saturated, then a queue forms upstream of the bottleneck, whose tail propagates upstream as a shock. In the same time, traffic emerges from the bottleneck accelerates in an expansion wave. After a while, all the commotion settles and an equilibrium state is reached, where a stationary queue forms upstream of the bottleneck, whose in/out flow rate equals the capacity of the bottleneck.

The third and fourth simulation runs are for the PW model, where we used the same initial conditions for density as in the first and second simulations, respectively, but different initial conditions for traffic speeds. These initial conditions (I.C.) are

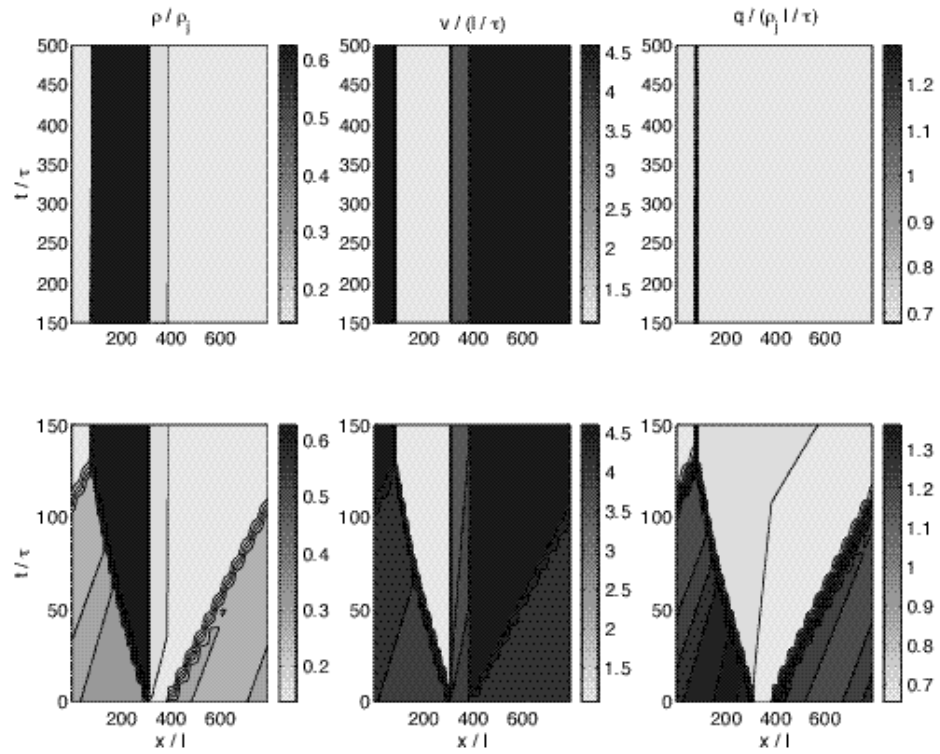

Figure 13: Solutions of the inhomogeneous LWR model with initial condition (116)

I.C. for the third simulation

$$\begin{aligned} a(x) &= 1, \quad x \in [0, L] \\ \rho(x,0) &= \rho_h + \Delta\rho_0 \sin\tfrac{2\pi x}{L}, \qquad x \in [0, L], \\ v(x,0) &= v_*(\rho_h, 1) + \Delta v_0 \sin\tfrac{2\pi x}{L}, \quad x \in [0, L]. \end{aligned} \tag{117}$$

I.C. for the fourth simulation

$$\begin{aligned} a(x) &= \begin{cases} 1, & x \in [320l, 400l) \\ 2, & \text{elsewhere} \end{cases} \\ \rho(x,0) &= a(x)(\rho_h + \Delta\rho_0 \sin\tfrac{2\pi x}{L}), \qquad x \in [0, L], \\ v(x,0) &= v_*(\rho_h, a(x)) + \Delta v_0 \sin\tfrac{2\pi x}{L}, \quad x \in [0, L]. \end{aligned} \tag{118}$$

The parameters are $\rho_h = 28$ veh/km, $\Delta\rho_0 = 3$ veh/km and $\Delta v_0 = 0.002$ km/s.

Again we use the same time step and cell size, which yields a CFL number of

$$\lambda_2 \frac{\Delta t}{\Delta x} \leq 0.9375 < 1$$

that ensures numerical stability of our finite difference approximation. The results of these simulation runs are shown in **Figure** 14 and **Figure** 15 respectively. Note that the PW model solution for the homogeneous road is slightly different that the corresponding LWR solution due to non-equilibrium initial speed, but the PW solution soon (about 10τ) looks very much like the LWR solution. This can be seen more clearly from time-slice plots of vehicle density, speed and flow rate shown in **Figure** 16. As can been seen from that figure, the solutions are nearly indistinguishable after $t = 140\tau$. In contrast, the PW solution for the inhomogeneous road, although shows similar patterns as the the corresponding LWR solution, does not converge to the LWR solution in long time (see **Figure** 15 & **Figure** 17). In long time, both solutions predict the same location of the tail anb head of the queue, but different discharge rate from the queue—traffic leaving the queue at capacity flow rate in the LWR solution, but below capacity flow rate in the PW solution (see **Figure** 17). This result highlights not only the differences between the two models, but also the importance and need for careful experimental validations of these models[6].

[6]The pikes in density that exceed jam density are possibly caused by traffic being unstable near the tail of the queue.

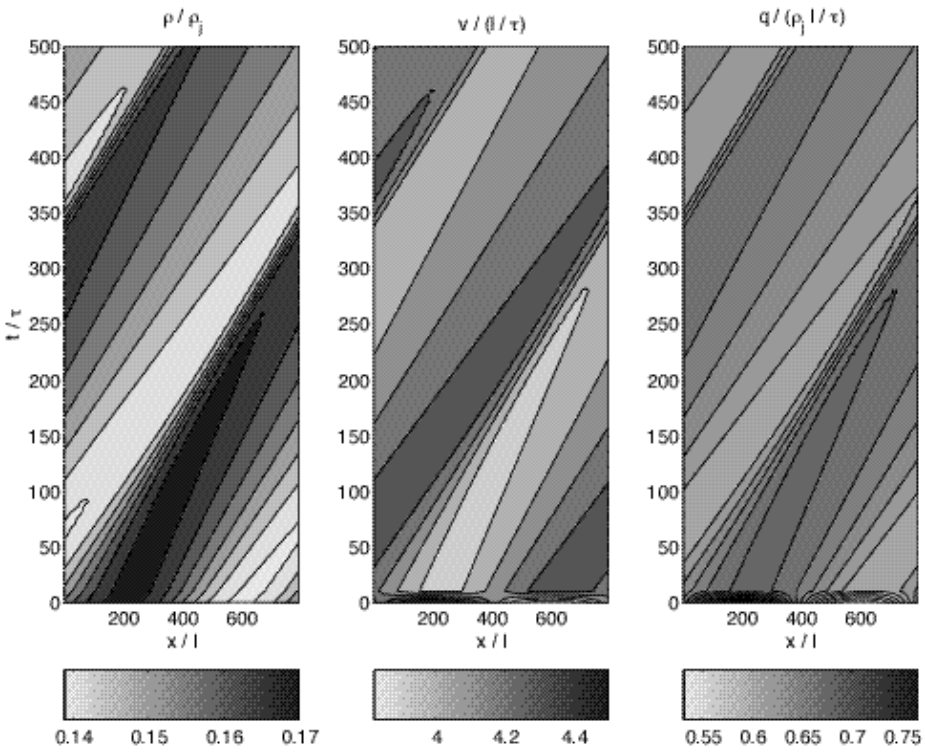

Figure 14: Solutions of the PW model with initial condition (117)

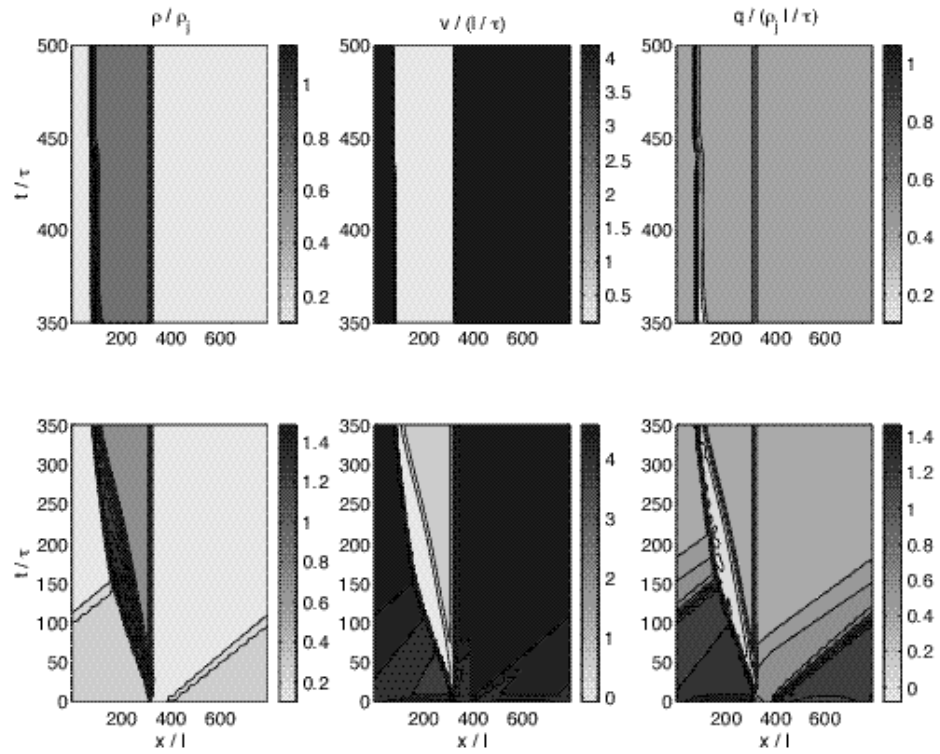

Figure 15: Solutions of the PW model with initial condition (118)

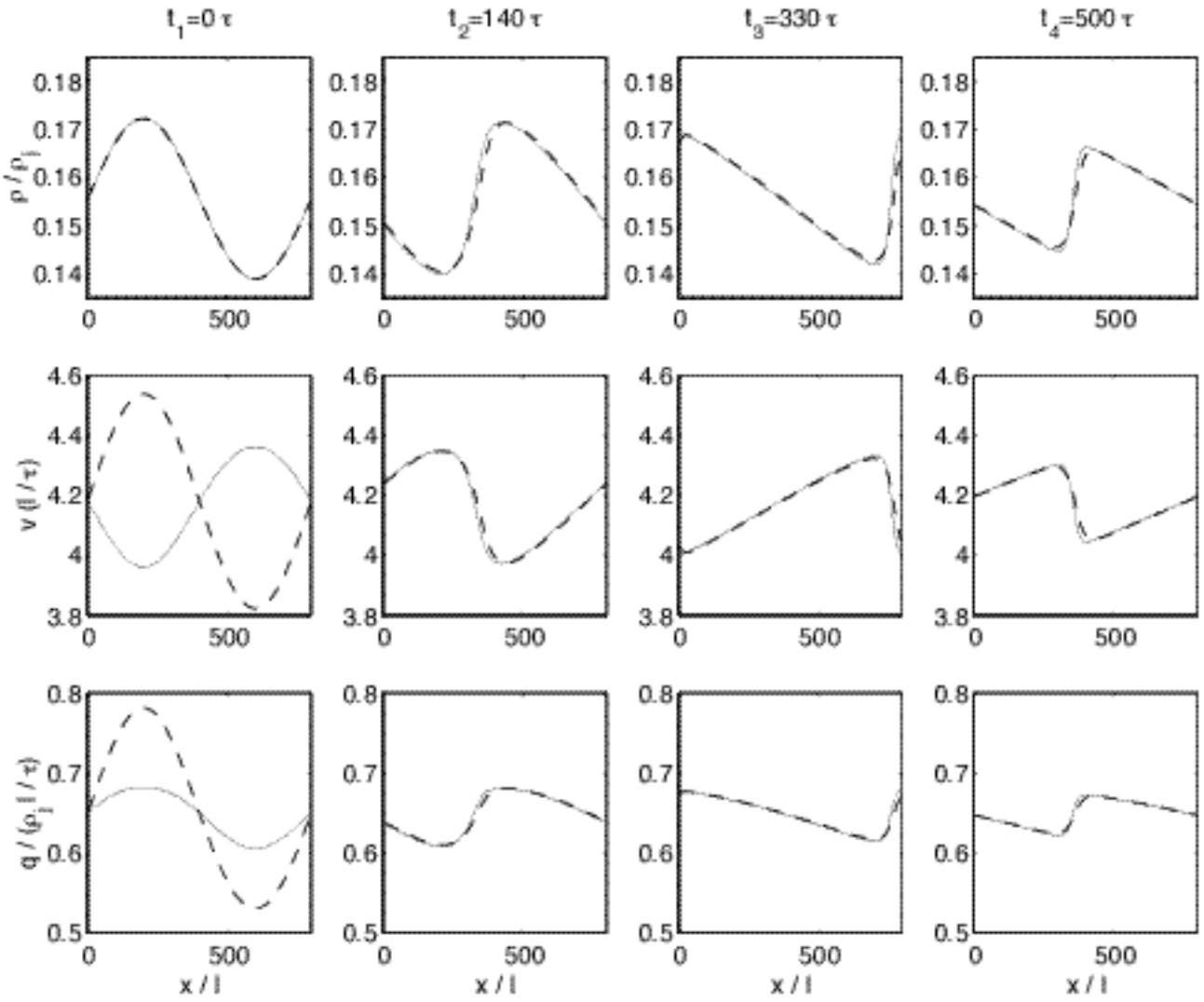

Figure 16: Comparison of the LWR model and the PW model on a homogeneous ring road: Solid line is used for the LWR model, and dashed line for the PW model

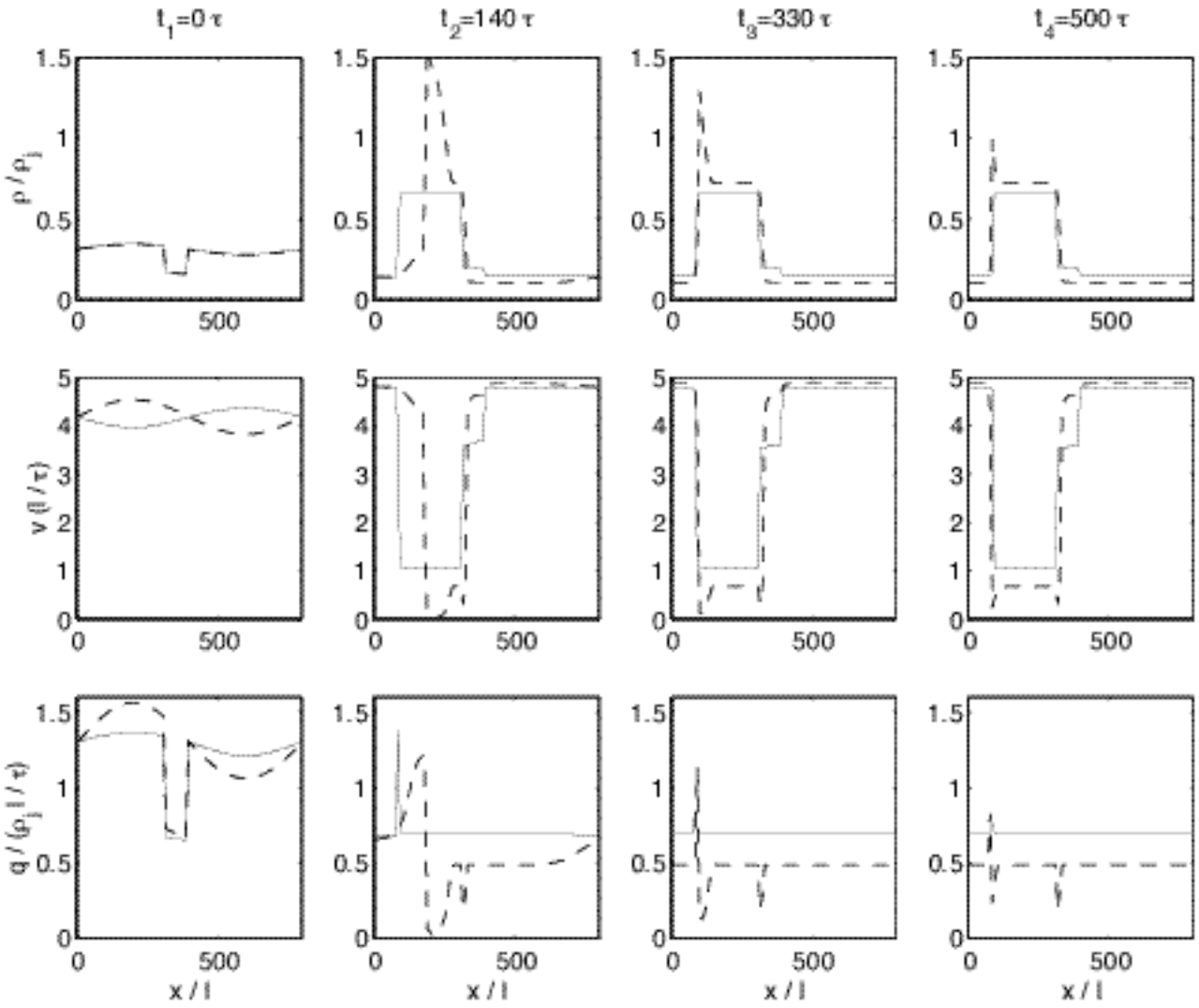

Figure 17: Comparison of the LWR model and the PW model on an inhomogeneous ring road: Solid line is used for the LWR model, and dashed line for the PW model

References

Bui, D., Nelson, P. & Narasimhan, S. L. (1992). Computational realizations of the entropy condition in modeling congested traffic flow, Technical Report, Texas Transportation Research Institute.

Courant, R. & Friedrichs, K. O. (1948) , *Supersonic flow and shock waves*, Interscience Publishers, Inc., New York.

Courant, R. and Hilbert, D. (1962). *Methods of mathematical physics*, Interscience Publishers, Inc., New York.

Cremer, M., F. Meiner, and S. Schrieber (1993). On Predictive Schemes in Dynamic Rerouting Strategies. In C. Daganzo (ed). *Theory of Transportation and Traffic Flow*, pp. 407-462.

Daganzo, C. F. (1994). The cell transmission model: a dynamic representation of highway traffic consistent with hydrodynamic theory, *Transpn. Res. B*, Vol. 28B, No.4, 269-287.

Daganzo, C. F. (1995a). Requiem for second-order approximations of traffic flow. *Transpn. Res. -B*, vol. 29B, No.4, 277-286.

Daganzo, C. F. (1995b). The cell transmission model, Part II: network traffic. *Transpn. Res. -B*, vol. 29B, No. 2, 79-93.

Daganzo, C. F. (1995c) , 'A finite difference approximation of the kinematic wave model of traffic flow', *Transportation Research, B* **29B**(4), 261–276.

Daganzo, C. F. (1997). *Fundamentals of Transportation and Traffic Operations*. Pergamon, Oxford.

Daganzo, C. F. (1999a). A Behavioral Theory of Multi-Lane Traffic Flow Part I: Long Homogeneous Freeway Sections, ITS Working Paper, UCB-ITS-RR-99-5.

Daganzo, C. F. (1999b). A Behavioral Theory of Multi-Lane Traffic Flow Part II: Merges and the Onset of Congestion", ITS Working Paper, UCB-ITS-RR-99-6.

del Castillo, J. M. Pintado, P. and F. G. Benitez (1994). The reaction time of drivers and the stability of traffic flow. *Transpn. Res.-B.* Vol. 28B, No. 1, 35-60.

del Castillo, J. M. and F. G. Benitez (1995). On functional form of the speed-density relationship—I: general theory, II: empirical investigation. *Transp. Res.* 29B, 373-406.

Dressler, R. F. (1949). Mathematical Solution of the Problem of Roll-Waves in Inclined Open Channels. *Commun. Pure and Appl. Math*, 2, 149-194.

Edie, L. C. and E. Bavarez (1967). Generation and propagation of stop-start traffic waves. In L. C. Edie, R. Herman and R. Rothery, eds., *Vehicular Traffic Science*, Elsevier, 26-37.

Gazis, D. C., R. Herman, and G. H. Weiss (1962). Density Oscillations Between Lanes of a Multilane Highway. *Oper. Res.*,10, 658-667.

Ferrari, P. (1989). The Effect of Driver Behaviour on Motorway Reliability. *Transportation Research, 23B*, 139-150.

Herrmann, M. and B.S. Kerner (1998). Local cluster effect in different traffic flow models, {em Physica A 255, 163-198.

Jin, W. L. and H. M. Zhang (2000a). The inhomogeneous kinematic wave traffic flow model as a resonant nonlinear system, submitted to *Transpn. Sci.*.

Jin, W. L. and H. M. Zhang (2000b). Numerical studies on the PW model, Working Paper, Institute of Transportation Studies, University of California at Davis.

Kerner, B. S. and Konhaüser, P. (1993). Cluster effect in initially homogeneous trafficflow, *Physical Review E* **48**(4), 2335–2338.

Kerner,B.S. and P. Konhäuser (1994). Structure and parameters of clusters in traffic flow, *Physical Review E* Volume 50, Number 1, 54-83.

Kerner, B. S., Konhaüser, P. and M. Shilke (1996). A new approach to problems of traffic flow theory. in: *Proceedings of the 13th Int. Symp. on Transportation and Traffic Theory*, J. B. Lesort, editor. 79-102, Pergamon, Oxford, U.K..

Kerner, B. S. and H. Rehborn (1999). Theory of congested traffic flow: self organization without bottlenecks. *Proceedings of the 14th Int. Symp. on Transportation and Traffic Theory*, Cedar, A., editor. 147-171, Pergamon, New York, NY.

Koshi, M., Iwasaki, M. and I. Ohkura (1983). Some findings and an overview on vehicular flow characteristics. *Proceedings of the 8th Int. Symp. on Transportation and Traffic Theory*, Hurdle, V., Hauer, E. and G. Stuart, editors. 403-451, University of Toronto Press, Toronto, Canada.

Kuhne, R. D. (1984). Macroscopic freeway model for dense traffic— stop-start waves and incident detection, *Ninth International Symposium on Transportation and Traffic Theory*, VNU Science Press, 20-42.

Kuhne, R. D. (1987). Freeway Speed Distribution and Acceleration Noise in N. H. Gartner, N. H. M. Wilson (eds.). *Proceedings of the Tenth International Symposium on Transportation and Traffic Theory*, Elsevier, 119-137.

Kuhne, R. D. (1989). Freeway control and incident detection using a stochastic continuum theory of traffic flow. In *Proc. 1st int. conf. on applied advanced technology in transportation engineering*, pages 287–292, San Diego, CA.

Kühne, R. D. and Beckschulte, R. (1993). Non-linearity stochastics of unstable traffic flow, *in* C. F. Daganzo, ed., 'Transportation and Traffic Theory', Elsevier Science Publishers., pp. 367–386.

Kühne, R. D. and K. Langbein-Euchner (1995). Parameter Validation. Report as an Order of Daimler-Benz Research, Stuttgart. Available by Steierwald Schnharting und Partner, Stuttgart.

Lax, P. D. (1972). *Hyperbolic systems of conservations laws and the mathematical theory of shock waves*, Society for Industrial and Applied Mathematics, Philadelphia, Pennsylvania.

Lebacque, J. P. (1996). The Godunov scheme and what it means for first order traffic flow models. *Proceedings of the 13th Int. Symp. on Transportation and Traffic Theory*, J-P Lesort, editor. 647-677, Pergamon, New York, NY.

Lebacque, J. P. (1999). Macroscopic traffic flow models: a question of order. *Proceedings of the 14th Int. Symp. on Transportation and Traffic Theory*, Cedar, A., editor. 147-171, Pergamon, New York, NY.

Leo, C. J., and R. L. Pretty (1992). Numerical simulations of macroscopic continuum traffic models. *Transpn. Res.-B.* 26B, No.3, 207-220.

Leutzbach, W. (1985). *Introduction to the Theory of Traffic Flow.* Springer Pub., 184-193.

Leutzbach, W. (1991) Measurements of Mean Speed Time Series Autobahn A5 near Karlsruhe, Germany. Institute of Transport Studies, University of Karlsruhe, Germany.

LeVeque, R. (1992) *Numerical methods for conservation laws*, Birkhäuser Verlag.

Lighthill, M. J. and Whitham, G. B. (1955). On kinematic waves: II. a theory of traffic flow on long crowded roads. In *Proc. Royal Society*, volume 229(1178) of *A*, 317–345.

Michalopoulos, P. G., Beskos, D. E. & Lin, J. K. (1984) , 'Analysis of interrupted traffic flow by finite difference methods', *Transportation Research, B* **18B**, 377–396.

Michalopoulos, P. G., D. E. Beskos, and Y. Yamauchi, (1984). Multilane Traffic Flow Dynamics: Some Macroscopic Considerations. *Transportation Research*, 18B, No. 4/5, pp. 377-395.

Michalopoulos, P. G., Jaw Kuan Lin, and D. E. Beskos, (1987). Integrated Modelling and Numerical Treatment of Freeway Flow. *Appl. Mathem. Model*, Vol. 11, No. 401, 447-458.

Michalopoulos, P. G., E. Kwon, and E. G. Khang, (1991). Enhancements and Field Testing of a Dynamic Simulation Program. *Transportation Research Record*, 1320, pp. 203-215.

Newell, G. F. (1961). Nonlinear Effects in the Dynamics of Car Following, *Operations Research, Vol 9*, pp.209-229.

Newell, G. F. (1965). Instability in dense highway traffic, a review. In Almond, P., editor, *Proceedings of the Second International Symposium on the Theory of Traffic Flow*, pages 73–85.

Newell, G. F. (1993). A simplified theory of kinematic waves in highway traffic, I general theory, II queuing at freeway bottlenecks, III multi-destination flows. *Transpn. Res. B*, Vol. 27, 281-313.

Papageorgiou, M., Blosseville, J., and Hadj-Salem, H.(1990) Modeling and Real-Time Control of Traffic Flow on The Southern Part of Boulevard Peripherique in Paris: Part I: Modeling, *Transportation Research, A*, 24 (5) 345-359.

Papageorgiou, M. (1998). Some remarks on macroscopic flow modeling. *Transportation Research, A*, 32 (5) 323-329.

Payne, H. J. (1971). Models of freeway traffic and control. In Bekey, G. A., editor, *Mathematical Models of Public Systems*, volume 1 of *Simulation Councils Proc. Ser.*, 51–60.

Payne, H. J. (1979). FREFLO: A Macroscopic Simulation Model of Freeway Traffic. *Transportation Research Record 722*, pp. 68-77.

Richards, P. I. (1956). Shock waves on the highway. *Operations Research*, 4:42–51.

Sailer, H. (1996). Fuid Dynamical Modelling of Traffic Flow on Highways–Physical Basis and Numerical Examples; Dissertation. (submitted for a Diploma) at the Institute for Theoretical Physics, University Innsbruck.

Treiterer, J. and J. A. Myers (1974). The hysteresis phenomena in traffic flow. *Proceedings of the sixth Int. Symp. on Transportation and Traffic Theory*, D. J. Buckley, editor. 13-38.

Verweij, H. D. (1985). Filewaarschuwing en Verkeer-safwikkeling. Ministry of Traffic and Water-Ways, Delft, The Netherlands.

Whitham, G. B. (1974). *Linear and nonlinear waves.* John Wiley & Sons, New York.

Zhang, H. M. (1998). A theory of nonequilibrium traffic flow. *Transportation Research, B*, 32(7):485–498.

Zhang, H. M. (1999). Analyses of the stability and wave properties of a new continuum traffic theory. *Transportation Research, B*, 33 (6) 399-415.

Zhang, H. M. and T. Wu (1999) Numerical simulation and analysis of traffic flow. *Transportation Research Record 1678*, 251-260.

Zhang, H. M. (2000a). Structural properties of solutions arising from a nonequilibrium traffic flow theory. *Transportation Research, B.* 34, 583-603 .

Zhang, H. M. (2000b). A finite difference approximation of a non-equilibrium traffic flow model. *Transportation Research, B.* (in press).

Zhang, H. M. (2000c). Anisotropic property revisited—when is it violated in traffic flow? Working paper, Institute of Transportation Studies, University of California at Davis (accepted for publication in *Trans. Res., -B*).

Zhang, H. M. (2000d). Phase transitions in a non-equilibrium traffic theory, " *ASCE Journal of Transportation Engineering*. Vol. 126, No. 1, 1-12.

Zhang, H. M. and T. Kim (2000). Effects of relaxation and anticipation on Riemann solutions of the PW model-a numerical investigation. *Transportation Research Record* (in press).

Zhang, H. M. (2001). New perspectives on continuum traffic flow models. *Special issue on traffic flow theory*, H. M. Zhang, ed., *Journal of Networks and Spatial Economics*, Vol. 1, Issue 1. 2001.